Chapter 4 Indium Tin Oxide Films Deposited by d.c. Sputtering

4.1. Introduction

Indium-tin-oxide (ITO) thin films are widely used in optoelectronics devices, flat panel display and electrochromic (EC) applications. The attractiveness of ITO is related to its low resistivity and high optical transmittance from visible to near infrared (NIR) light. However, these properties are strongly dependent on the growth conditions such as ratio of oxygen partial pressure P_{02}, bias voltage, substrate temperature (T_s) and post annealing. It is well known that high quality ITO film is easily obtained at high T_s (>300 ^{0}C) using most of the deposition techniques available [1-3]. Therefore an improvement of the method to grow ITO film at low T_s or room temperature (RT) is needed in order to avoid annealing in industrial production. This is due to the fact that in flat panel displays EC window applications, the organic colour filters, heat sensitive layers such as polymers and others (CdS, electrolytes etc.) are used. Many of these different layers do not sustain higher process temperatures [3-5].

Higher transmission and smaller as possible sheet resistance (R_s) are very important for the applications of smart EC window. The extensive use of ITO films had led to researches on various deposition techniques. Reactive ion plating [6], d.c. diode sputtering [7], r.f. sputtering [8], reactive evaporation [9-10], electron beam [11], chemical vapour deposition and spray pyrolysis [12] have all been used to deposit transparent conducting film. Though many deposition techniques have been used, among the techniques for ITO thin film production, sputtering is the most widely investigated and large-scale deposition setups are available [7-8, 13]. We chose to deposit ITO films by the dc-magnetron sputtering method, because a high sputtering rate and good film performances and low cost deposition system could be achieved comparing with a r.f. sputter system.

As we know, there are two basic kinds of sputtering techniques: radio frequency (r.f.) sputtering and direct current (d.c.) sputtering (Chapter 2). In our previous study[8] r.f. diode sputtering was used for the deposition of ITO by ceramic target without substrate

heating. The lowest sheet resistance of ITO film attained without annealing, was about 48 Ω/Sq. at 300 nm thickness and a maximum visible transmission of about 81 %. In this work we present the study of d.c. sputter ITO films obtained by a ceramic target by varying $P_{02,}$ bias voltage, substrate temperature and post annealing.

4.2. Influence of P_{O2} on the Properties of ITO Films at Room Temperature

ITO films with different oxygen partial pressure ratio (P_{O2}: from 27% to 0) were prepared with a sputtering atmosphere of $2.1x10^{-1}$ Pa total pressure (P_T). In Table 4-2-1 an overview of the results is shown.

Table 4-2-1. Deposition conditions and parameters of ITO films

Samp.	P_{O2}	T_d (Min.)	d_e (nm)	T_{max} (%)	R_s (Ω/Sq.)	δ (nm)	E_g (eV)	Φ_{max} ($10^{-3}\Omega^{-1}$)
a1	27%	0.7	-	99.6	∞	13.6	-	-
a2	25%	0.7	-	99.5	∞	13.2	3.53	-
a3	21%	0.7	-	99.3	760.2	11.2	3.49	1.3
a4	16 %	2	48	97.0	654.0	12.2	3.48	1.5
a5	12 %	2	94	95.0	108.7	11.5	3.53	8.7
a6	10 %	2	91	95.0	99.9	12.2	3.62	9.4
a7	2%	2	66	94.0	132.8	13.6	3.66	7.1
a8	0	2	-	93.0	137.6	11.9	3.26	6.8

Note. Samp.: sample; P_{O2}: ratio of oxygen partial pressure; $T_{d:}$ deposition time; d_e: thickness obtained by fitting of ellipsometric parameter; T_{max}: transmittance at maximum; R_s: sheet resistance; δ: Surface roughness; E_g: Energy band gap; Φ_{TC}: Figure of Merit.

4.2.1. Transmission spectra of ITO films

The transmission spectra of some as-deposited ITO films are shown in Fig. 4-2-1. All maximum transmission (T_{max}) data of the samples is listed in Table 4-2-1. A T_{max} of about 99 % is achieved in the visible spectral region for a1, a2 and a3 samples. The transmission curves in the long wavelength (NIR: near infrared) region shift to red direction and increases with increasing P_{O2} except for the lowest P_{O2} sample (2%). This

indicates an increase of the amount of free electrons in the films with decreasing P_{O2}, because the electrons are from oxygen vacancies in ITO film [13, 16].

The optical properties of ITO films are determined to a large extent by the microstructure of the film and hence by the preparation technique. It is believed that the decrease of the transmittance at lower P_{O2}, which is smaller than the optimum 10% P_{O2}, is due to formation of non-stoichiometric films. As P_{O2} is increased, the film structure may also vary from a dense structure into a columnar (Section 9.4) or cluster structure with more pronounced voids. All these could result in an increase in transmittance. All values of the transmission of as-deposited ITO films are above 83% in the range (470 nm to 1900 nm). From Table 4-2-1 the optimum depositing conditions of 10% and 12% P_{O2} result in a high transmission of 95 % with lowest R_s. Although this value of transmittance is not as high as that of sample a1 (27% P_{O2}), it is good enough for application.

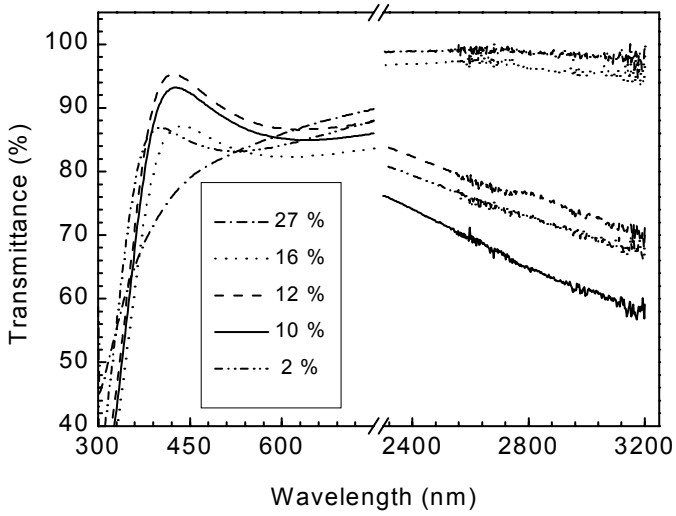


Fig. 4-2-1. Transmittance spectra of films prepared with different oxygen partial pressure ratio.

4.2.2. Sheet resistance

The lowest value of the sheet resistance (R_s) of the ITO films was attained with 2 minutes deposition time (T_d), and it is 99.9 Ω/ Sq. (Ohm/Square) for 10% P_{O2}. Other R_s of ITO films are 132.8 Ω/ Sq. for 2% P_{O2}, 137.6 Ω/ Sq. for 0 P_{O2}, 108.7 Ω/ Sq. for 12% P_{O2} and 654.0 Ω/ Sq. for 16% P_{O2} respectively. An increase in R_s on either side of the optimum 10% P_{O2} was observed after increasing and decreasing P_{O2}. At lower than the optimum P_{O2} the film resulted in higher R_s, which is due to the formation of non-stoichiometric films. At higher values than the optimum P_{O2} values the larger R_s could

be due to additional oxygen accumulated at the grain boundaries that acts as scattering centres to electrons. From the above, the R_s of the as-deposited ITO film is sufficiently low to use as an electrode layer. In table 4-2-1 the R_s of the ITO films as a function of P_{O2} in the sputtering atmosphere is shown.

4.2.3. Figure of Merit

Table 4-2-1 shows the maximum value of Figure of Merit ($\Phi_{TC}= T/R_s$) of the films and the best one with the lowest R_s, is sample a6, Φ_{max} (T_{max}/R_s) = 9.4 x 10^{-3} Ω^{-1}. Φ_{TC} is mainly influenced by R_s, because of its definition expression, as follows [1, 16-18].

$$R_s= \rho/d. \qquad (4.2.1)$$

$$T= (1-R)^2 e^{-\alpha d} . \qquad (4.2.2)$$

$$\Phi_{TC} (\lambda) =T/ R_s = d (1-R)^2 e^{-\alpha d}/\rho. \qquad (4.2.3)$$

Where ρ is the resistivity, d is the thickness of film and R is the reflectance. T and α are the transmittance and absorption at a particular wavelength. Clearly, increasing the thickness of the ITO films has a strong influence on the R_s, but it does not affect the transmittance so much.

4.2.4. Surface roughness (δ) and TIS of the films

Generally the carrier scattering in a rough surface of the film may be affected to the electrical conduction of a very thin ITO film. In most cases surface roughness (δ) is an important parameter of the thin film. The surface morphology of the ITO films is not given by using SEM, because the film is too smooth to be observed using a normal SEM. Here a spectrum method was used to study the surface morphology. Fig. 4-2-2 shows the diffuse reflectance, specular reflectance and TIS spectra of the ITO films over a wavelength range of 300-810 nm. The δ values based on Equ.(3.2) in Section 3.3, for all samples, are summarized in Table 4-2-1. Fig. 4-2-3 is a typical AFM micrograph of the surface microstructure and topography of the ITO film deposited at RT and 10% P_{O2}. As seen in Table 4-2-1 the surface has roughness from 11.2 nm to13.6 nm. A little rougher surface was obtained for larger P_{O2} (27%) and less P_{O2} (2%). As we know the light scattering can be caused by the surface δ and the grain boundaries. The δ surface and nanometer grain boundaries are clearly seen by AFM in Fig.4-2-3. The grain size is 30 nm and the average height of δ is less than 15 nm. Because the prepared ITO sample is a good transparent thin film, we suppose that the scattering mainly comes from the interface of the film.

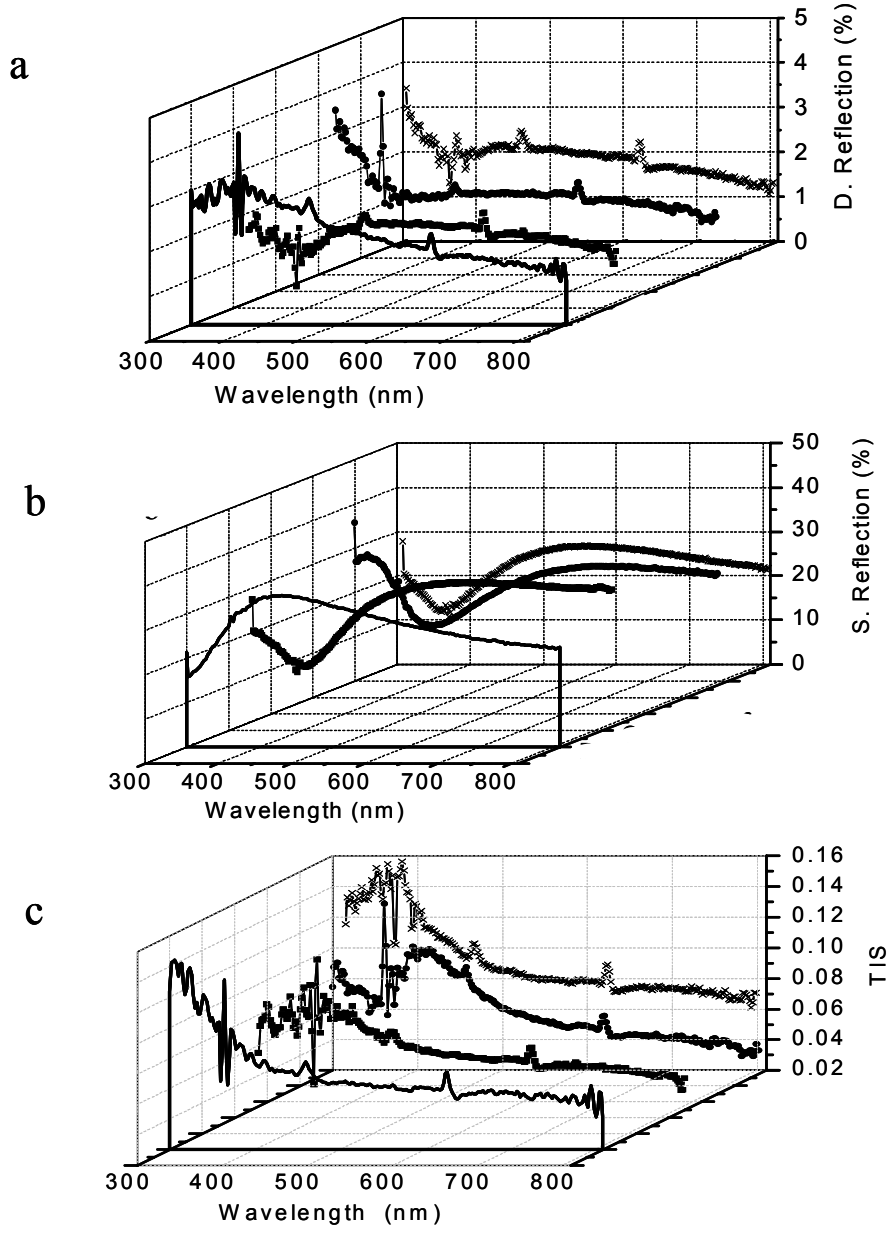


Fig. 4-2-2. (a)Diffuse reflectance, (b)specular reflectance and (c)TIS spectra of ITO films over a wavelength range of 300-810 nm in different oxygen partial pressure (P_{O2}). Solid line: 27% $P_{O2,}$ Square: 16% $P_{O2,}$ Circle: 10% $P_{O2,}$ Cross: 2% $P_{O2.}$

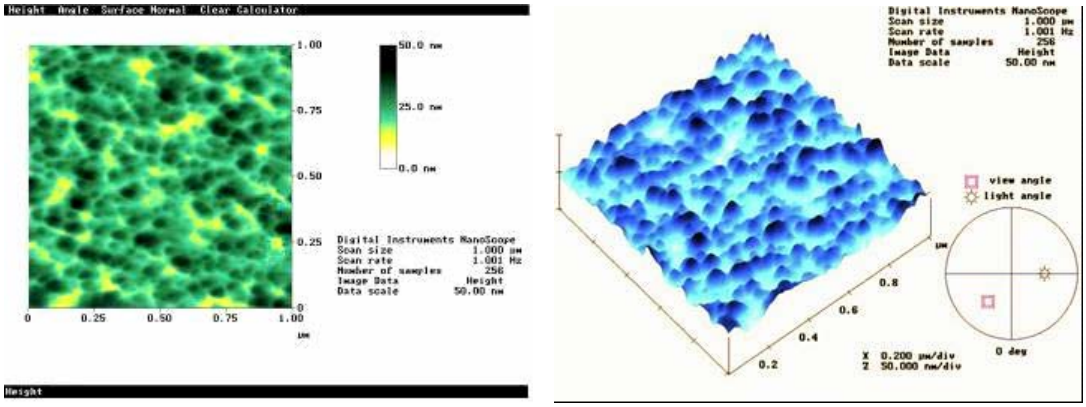


Fig. 4-2-3. AFM surface microstructure and topography of an ITO film (sample a6) at 10% ratio of oxygen partial pressure.

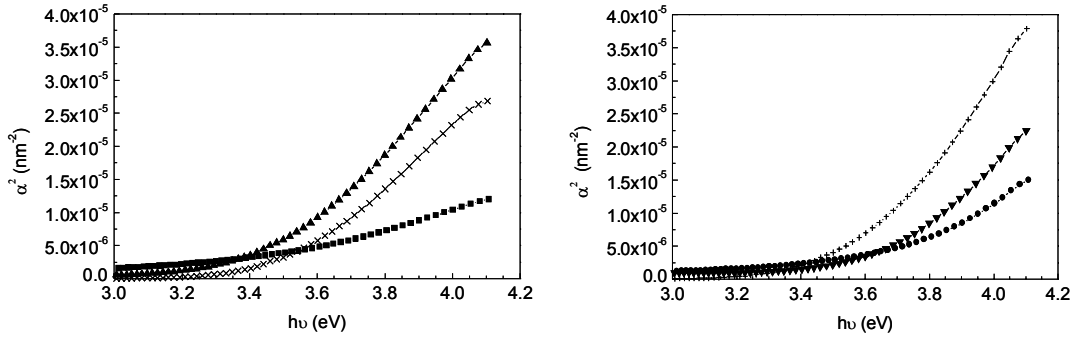


Fig. 4-2-4. Dependence of the absorption coefficient on the photon energy. Square: 27% P_{O2}: Up triangle: 16% $P_{O2,}$ Cross x: 12% P_{O2}, Circle: 10% P_{O2} (4 Min.), Cross+: 10% P_{O2} (2 Min.), Down triangle: 2% P_{O2}

4.2.5. Energy band gap (E_g)

There are different models and many reports about the absorption coefficient and energy band gap (E_g) [13]. Here we gave the calculated E_g values using the direct transition model (N=2) by $\alpha^N = C (h\nu - E_g)$ (Section 3.7). α^2 are plotted vs. the photon energy (Fig. 4-2-4), which is obtained from measurements of the absorption spectrum. Extrapolating the linear region towards the hν axis gives the effective Eg. Table 4-2-1 shows the E_g values of the ITO films.

The intrinsic Eg of the ITO material is 3.53 eV [19]. The obtained values of the films vary between 3.26 and 3.66 eV. As some of the ITO films (samples a6 and a7) treated in this work show comparably high effective $E_{g,}$ possibly this is caused by a combination of Burstein-Moss-Shift [20] and contributions of scattering [21]. It should be as following, $E_g = E_{g,0} + \Delta E_{BM} = E_{g,0} + \hbar (3\pi^2 n_e)^{2/3}/2m^*_{vc} + \hbar\Sigma$, Where E_g is the

measured or varied effective band gap, $E_{g,0}$ is the intrinsic band gap, m^*_{vc} represents the reduced effective mass and n_e is free electron density. The $\hbar\Sigma$ represents the broadening of the band gap due to scattering and widening of the transition. It is assumed that the Sn^{4+} ions behave as single charged point scatter too except the boundary scatter. We can see that the ΔE_{BM} value comes from the contribution of both $\hbar\Sigma$ and $\hbar (3\pi^2 n_e)^{2/3}/2m^*_{vc}$. For other samples that have comparably low effective E_g (<3.53 eV), it is possibly caused by the structure of non-stoichiometric sample when the ITO films were deposited at higher or lower P_{O2}. From above discussion the variant E_g value of the ITO film is not explained by only a Burstein-Moss-Shift like Bender et al mentioned [13].

4.2.6. Conclusions of the section

Transparent and conductive ITO films were deposited on glass using dc-magnetron reactive sputtering at room temperature (RT) with different P_{O2}. The effects of P_{O2} on the ITO films were discussed. The lowest R_s was obtained for ITO film with 10% P_{O2}, and after increasing P_{O2} a rapid decline in the R_s occurred. For the optimum sample a6, the film with 91 nm thickness has 99.9 Ω/Sq sheet resistance, 95% maximum visible transmission and 9.4×10^{-3} Ω^{-1} Figure of Merit (Φ_{TC}). From AFM results and spectra calculations, the δ values of the ITO films were analysed and are lower than 15 nm. The energy band gap E_g varies within 3.26 eV - 3.66 eV and increases as the P_{O2} decrease in the range of 20% - 2% P_{O2}. The high value of E_g of the film under consideration compared to the intrinsic E_g could be explained by a modified Burstein-Moss-Shift. No post annealing was done in the production process of the film. This is a less expensive and more practical for some device applications.

4.3. Influence of Negative Bias Voltage on the Properties of ITO Films

4.3.1. Electrical properties of the ITO films

In Table 4-3-1 an overview of the sheet resistance (R_s), transmittance and other parameters of samples investigated in the following sub-sections are shown. The lower R_s value of the ITO film is 143.6 Ω/square, which corresponds to the sample that was deposited at –70 V bias, 300 ^{0}C heated substrate, and 1.1×10^{-1} Pa total pressure for 0.7 minutes coating time. Comparing these samples both heated and no heated substrate with negative bias voltage can clearly improve the conductivity of the film.

Table 4-3-1. Experimental conditions and parameters of the ITO films deposited with variable bias voltages and substrate temperatures with 21% ratio of oxygen partial pressure.

Samp.	P_{O2} (%)	T_d (Min.)	T_{max} (%)	R_s (Ω/ Sq.)	E_g (eV)	Φ_{max} ($10^{-3}\Omega^{-1}$)	note
b1	21	0.7	99.3	760.2	3.49	1.3	RT, no bias
b2	21	0.7	98.1	254.3	3.38	3.9	RT, -40V bias
b3	21	0.7	97.5	240.0	3.39	4.1	RT, -70V bias
b4	21	0.7	97.5	238.6	3.54	4.1	RT, -100V bias
b5	21	0.7	97.9	209.8	3.59	4.6	100 ^{0}C Sub., -100V bias
b6	21	0.7	98.0	145.8	3.65	6.7	200 ^{0}C Sub., -100V bias
b7	21	0.7	98.0	143.6	3.68	6.8	300 ^{0}C Sub., -100V bias
b8	21	5	92.5	33.2	3.77	27.9	RT, -100V bias

Symbols and abbreviations refer to Table 4-2-1.

4.3.2. Optical properties of ITO films

Transparency of the films is affected by absorption, reflection, and scattering losses. These losses are related to the microstructure and surface roughness of the films. The following section will give the results of their study.

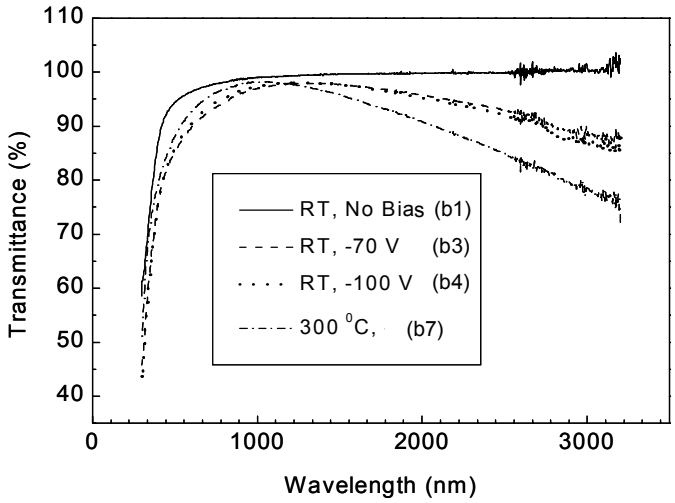


Fig. 4-3-1 Transmittance spectra of the films prepared with different bias voltages and substrate temperatures for the samples with 21% ratio of oxygen partial pressure and 1.1×10^{-1} Pa total pressure.

a. Transmission spectra

The transmission spectra of some ITO films are shown in Fig.4-3-1. All ITO transmittance data at maximum (T_{max}) is listed in Table 4-3-1. About 99.3 % T_{max} is achieved in the visible spectral region for sample b1 and 98% for most samples. The transmission behaviour shifts to red direction in the long wavelength region and decreases with increasing negative bias voltage and substrate temperature. This indicates an increase of free electrons in the films with variation of bias voltage and substrate temperature [16].

b. Diffuse and specular reflectance spectra

Fig. 4-3-2 shows the diffuse reflectance (DR) and specular reflectance (SR) for different negative bias voltage and substrate temperature of the films as a function of wavelength. The intensity variation with wavelength of SR is similar to that of DR. The intensity of sample b1 is the lowest. The specular reflectance decreases when the negative bias voltage and substrate temperature increases. This leads to the increase of transmittance in visible region for the samples with bias. Sample b1 has the better transmittance. The influence of the negative bias in the film structure will be detailedly discussed in Section 7.3.3. Using the above specular and diffuse reflectance spectra, the surface roughness (δ) can be obtained by the TIS method (Section 4.2.4 and Section 3.3). The δ values for all the samples are lower than 10 nm.

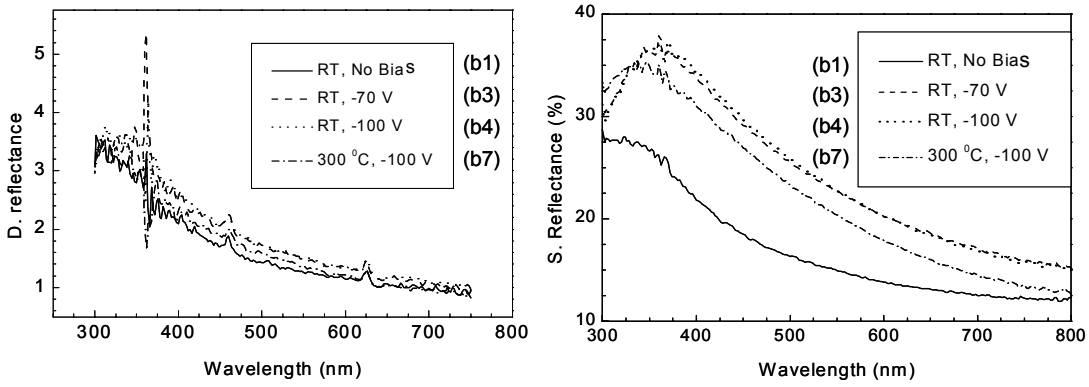


Fig. 4-3-2. Diffuse reflectance (DR) and specular reflectance (SR) for different bias voltage and substrate temperature, as a function of wavelength.

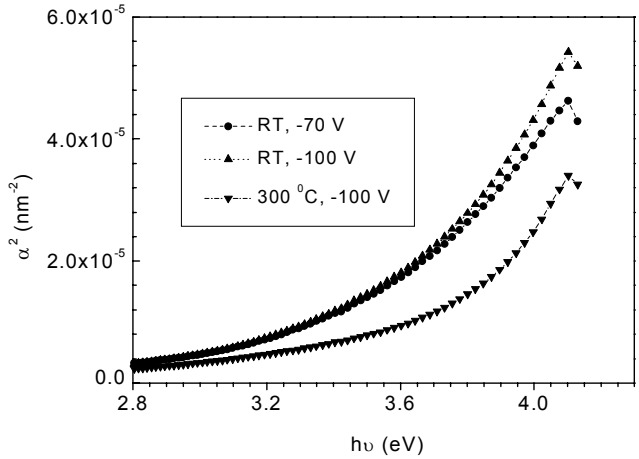


Fig. 4-3-3. Dependence of the absorption coefficient on the photon energy.

c. Energy band gap (E_g)

Here we give the calculated E_g values by using the direct transition model (N=2) ($\alpha^N = C(h\nu - E_g)$, see Section 3.7). α^2 is plotted vs. the photon energy (Fig. 4-3-3), which is obtained from measurement of the absorption spectrum. Table 4-3-1 shows the E_g values of the ITO films. The obtained E_g values vary between 3.38 and 3.77 eV for films deposited with different bias voltage and T_s. As the sample b5-b8 show comparably high E_g comparing with the intrinsic E_g =3.53 eV, we conclude that this is mainly caused by a large Burstein-Moss-shift (Section 4.4.4) [20].

4.3.3. Conclusion of the section

The ITO thin films were deposited on glass with different negative bias voltages. The electrical properties of the film are strongly dependent on the deposition conditions. There is an improvement of the film electrical properties after increasing the negative bias voltage and substrate temperature. The film that was deposited at RT without bias has the best transmission (T_{max}: 99.3 %). For the optimum sample (b7) deposited in 0.7 minutes (thickness: 45 nm), the sheet resistance is 143.6 Ω/Sq, the maximum transmission is 98% and Figure of Merit (Φ_{TC}) is 6.8×10^{-3} Ω^{-1}. For 5 minutes deposition time the film is much thicker and has much lower R_s. The surface δ of the ITO film was analysed. The E_g varies within 3.38 eV – 3.77 eV. The high values of E_g

of the films under consideration compared to the intrinsic Eg could be mainly explained by the Burstein-Moss-Shift.

4.4. Influence of Heated Substrate on the Properties of the ITO Films

4.4.1. Electrical properties of ITO films

Table 4-4-1 shows an overview of the sheet resistance (R_s), transmittance and other parameters of samples investigated in the following sub-sections. The lowest R_s value of a good transparent ITO film is 89.9 Ω/Sq. It was deposited at 400 ^{0}C substrate temperature (T_s), 0.7 minute deposition time (T_d) and 1.1 x 10^{-1} Pa total pressure. Other R_s of ITO films are 206.3 Ω/Sq for 400 ^{0}C T_s at only 0.35 minute T_d and 173.6 Ω/Sq for 350 ^{0}C T_s. Comparing all samples the heating of the substrate can clearly improve the conductivity of the films.

Table 4-4-1. Experimental conditions and parameters of the ITO films deposited with 21% ratio of oxygen partial pressure (Symbols and abbreviations refer to Table 4-2-1).

Samp.	T_d (Min.)	d_e (nm)	T_{max} (%)	R_s (Ω/ Sq.)	E_g (eV)	Φ_{max} ($10^{-3}\Omega^{-1}$)	T_s (^{0}C)
c1	0.7	40	99.5	760.2	3.49	0.27	RT
c2	0.8	48	97.5	417.4	3.68	2.3	150
c3	0.8	46	97.5	412.6	3.59	2.4	200
c4	0.7	39	97.8	238.6	3.54	4.1	300
c5	0.7	43	98.0	173.6	3.69	5.6	350
c6	0.7	55	98.2	89.9	3.64	10.9	400
c7	0.35	24	99.6	206.3	3.68	4.8	400
c8	32	5000	-	3.9	-	-	400

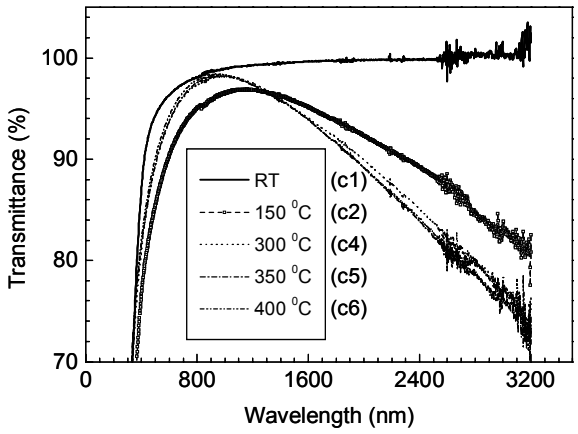


Fig. 4-4-1. Transmission spectra of films prepared with different substrate temperature at 21 % ratio of oxygen partial pressure and 1.1 ×10^{-1} Pa total pressure.

4.4.2. Transmission spectra

The transmission spectra of some ITO films (Sample c1, c2, c4, c5, c6) are shown in Fig.4-4-1. All transmission data of the samples at maximum are listed in Table 4-4-1. The maximum transmission of about 97%~99 % is achieved in the visible spectral region. The transmission behaviour shifts to red direction and increases with decreasing substrate temperature in the long wavelength region. This indicates an increase of free electrons in the films with increase of substrate temperature [16].

4.4.3. Diffuse and specular reflectance spectra.

Fig. 4-4-2 shows the diffuse reflectance (DR) and specular reflectance (SR) for different substrate temperature (T_s) of the films, as a function of wavelength. The intensity of sample c1 (RT deposition) is much weaker than other samples (heated substrate deposition). The intensity of sample c2 (150 ^{0}C T_s) is stronger than other samples. The lower SR of sample c1 leads to the increase of the transmittance of the film. Using the above specular and diffuse reflectance spectra, the surface roughness (δ) can be obtained by the TIS method (Section 4.2.4). The δ values calculated based on Equ.(3.2) (Section 3.3) for all samples are lower than 8 nm.

Fig. 4-4-3 shows typical AFM micrographs of the surface microstructure and topography of the ITO film (sample c6) deposited with 21% P_{O2} and 400 ^{0}C substrate temperature. A rough surface and larger grain boundaries are clearly seen in Fig.4-4-3. The average grain size is 130 nm and the average height of δ is less than 5 nm. Comparing with the AFM picture of sample a6 (thickness: 91 nm, grain size: 30 nm, Section 4.2), the sample c6 has much bigger grain size. The larger grain or domain in the film, decreases free electrons scattering by the grain boundaries, which results in a much lower R_s.

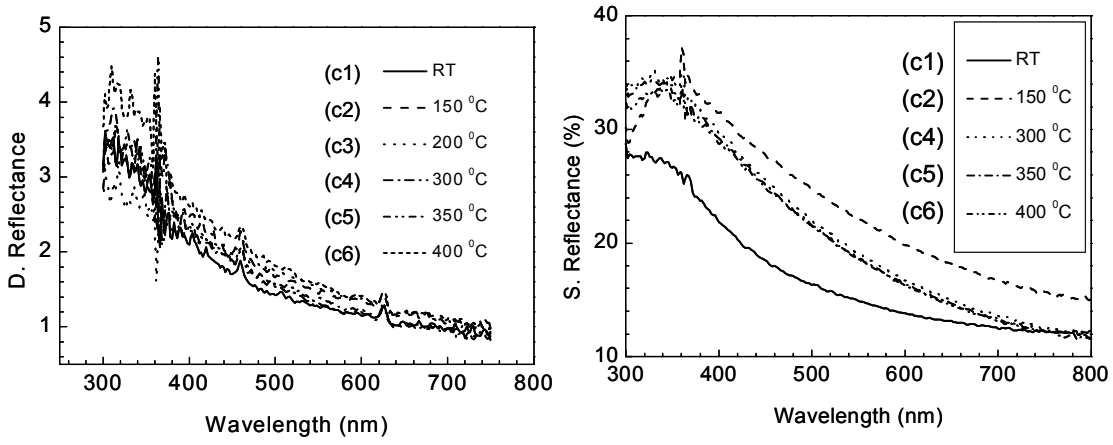


Fig. 4-4-2. Diffuse reflectance (DR) and specular reflectance (SR) for different substrate temperatures as a function of wavelength.

4.4.4. Energy band gap (E_g)

Similar to Section 4.3.2, Table 4-4-1 and Fig. 4-4-4 show us E_g values of the ITO films. The obtained E_g values vary between 3.49 and 3.69 eV with different T_s. The comparably high E_g of the ITO samples is possibly caused by the Burstein-Moss-Shift [20]. $E_g = E_{g,0} + \Delta E_{BM} = E_{g,0} + \hbar (3\pi^2 n_e)^{2/3}/2m^*_{vc}$, Where E_g is the measured or varied effective band gap, $E_{g,0}$ is the intrinsic band gap, m^*_{vc} represents the reduced effective mass and n_e is free electron density. We can see that the ΔE_{BM} value comes from the increased electron density in the high temperature deposition.

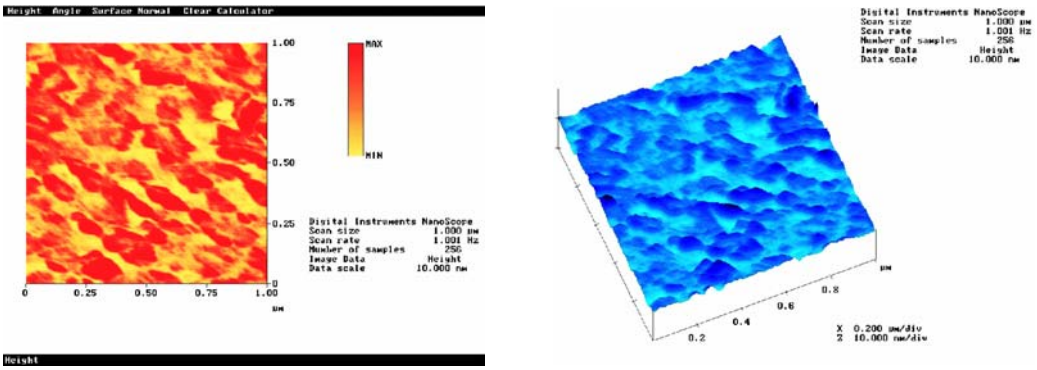


Fig. 4-4-3. AFM surface microstructure and topography of an ITO film (sample c6) deposited at 21% ratio of oxygen partial pressure and 400 ^{0}C substrate temperature.

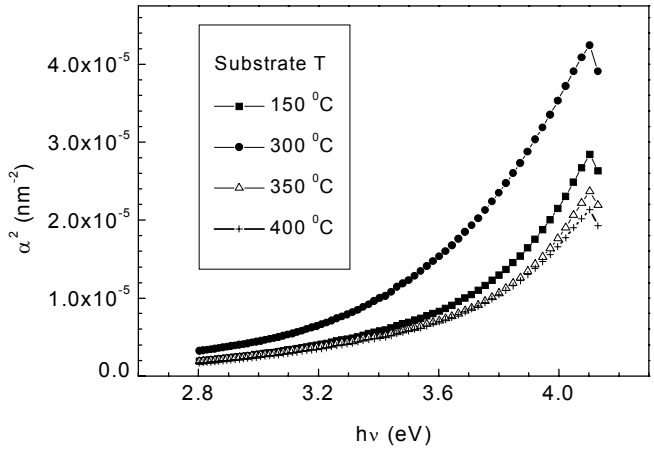


Fig. 4-4-4. Dependence of the absorption coefficient on the photon-energy.

4.4.5. Structural characteristics

The microstructure of metal oxide film prepared by sputtering is not the same for films prepared at different deposition conditions [23]. Fig. 4-4-5 shows the XRD curve of

the ITO film deposited at 400 ^{0}C substrate temperatures (Sample c6). An amorphous film was obtained, irrespective of the SnO_2-doping concentration in the film. The prepared ITO film has no sharp peaks in the X-ray diffraction spectrum. Only a weak peak of In_2O_3 (211), a mixing peak of In_2O_3 (222) /$In_2Sn_2O_{7-x}$ (222), In_2O_3 (421), In_2O_3 (440) and In_2O_3 (622) plus a broad background from the glass substrate can be observed. This is because the film was amorphous and the film was thin. There is no evidence of the pure SnO_2 in the spectrum. This could be caused by the small amount of SnO_2 phase in the thin ITO film and the low resolution of the experimental system. Comparing the XRD of the ITO film without substrate heating (deposited at RT) in Fig. 4-7-3, the XRD of sample c6 has extra peaks In_2O_3 (421), In_2O_3 (440) and In_2O_3 (622). A more detailed discussion is given in Section 4.7.5.

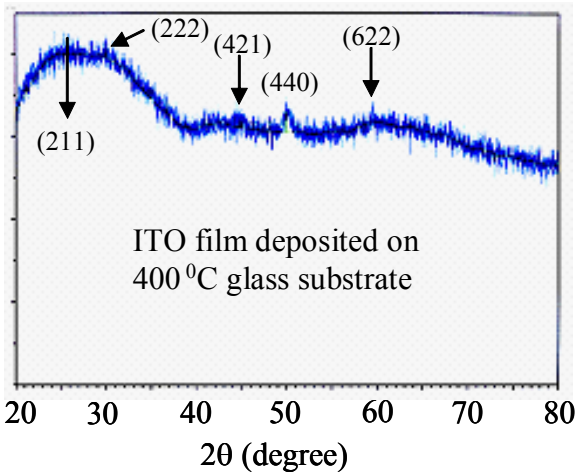


Fig. 4-4-5 XRD pattern of ITO film on a glass substrate, deposited at 400 ^{0}C temperatures.

4.4.6. Conclusion of the section

The ITO thin films were deposited at different substrate temperatures. The electrical properties of the films show strongly dependence on T_s. There are clear improvements of the film electrical properties after increasing substrate temperature during deposition. For the optical properties, the transmission has not a clear change in the visible range. For the optimum sample (c6), the film has 89.9 Ω/Sq sheet resistance, 98.2% maximum visible transmission, and 10.9×10^{-3} Ω^{-1} Figure of Merit (Φ_{TC}) at 55 nm thickness. For 32 minutes deposition time the film (sample c8) is much thicker and has much lower R_s. The surface δ of the ITO film was calculated by the TIS method and analysed by AFM. The δ values of the films are less than 8 nm. The E_g varies within 3.49 eV – 3.69 eV with substrate temperature. The high E_g values of the films could be mainly explained

by Burstein-Moss-Shift. An amorphous ITO film was obtained even if it was grown at more than 400 ^{0}C substrate temperatures. It suits to fabricate ECDs based on WO_3 film, because this amorphous ITO film matches well with amorphous EC WO_3 film.

4.5. Influence of thickness on the Properties and Microstructure of the ITO Films

4.5.1. Transmission of ITO films

The transmission spectra of as-deposited ITO films are shown in Fig. 4-5-1. All data of the transmittance at maximum (T_{max}) is listed in Table 4-5-1. The transmission decreases and the spectral range narrows with increasing thickness (or with increasing deposition time). All values of transmission of as-deposited ITO films are above 75% in visible range (wavelength more than 400 nm) except samples d5 and d7 that were deposited in more than 18 minutes. The transmission curves become lower at NIR range. In addition, the transmission behaviour in the long wavelength region (NIR) shifts towards shorter wavelength with increasing thickness. This indicates an increase of free electrons in the film [13]. From Table 4-5-1 the optimum 94% maximum visible transmission is found for nearly all samples. A more detailed discussion on the relation of structure and transmission will be further given in section 4.5.6.

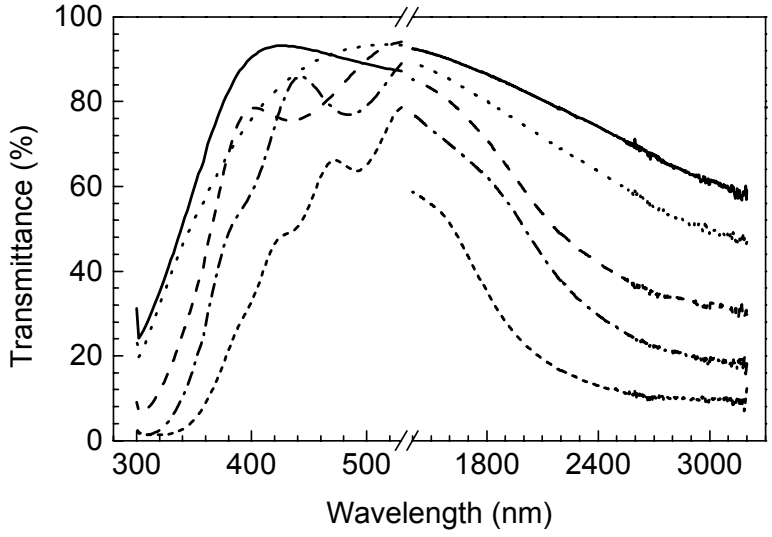


Fig. 4-5-1. Transmittance spectra of films prepared with 10% oxygen partial pressure and 2.1 x 10^{-1} Pa total pressure for different deposition time. Solid line: 2 Min. (d1 sample), Dot line: 4 Min.(d2), Dash line: 6 Min. (d3), Dash dot line: 10 Min. (d4), Short dash line: 18 Min. (d5).

Table 4-5-1. Deposition conditions and parameters on the ITO films

Samp.	P_{O2} (%)	T_d (Min.)	d (nm)	T_{max} (%)	R_s (Ω/ Sq.)	δ (nm)	E_g (eV)	Φ_{max} ($10^{-3}\Omega^{-1}$)
d1	10	2	97	94	99.9	12.2	3.62	9.4
d2	10	4	188	94	85.6	11.4	3.69	11.0
d3	10	6	282	94	32.5	12.4	3.58	28.9
d4	10	10	470	94	26.5	11.3	3.56	35.1
d5	10	18	846	90	20.8	11.6	3.32	44.2
d6	21	2	152	96	139.1	12.9	3.59	6.9
d7	21	32	5000	-	3.9	-	-	-

Symbols and abbreviations refer to Table 4-2-1.

4.5.2. Sheet Resistance and Figure of Merit

In table 4-5-1 the R_s of ITO as a function of thickness is shown. A slight decrease in R_s is observed with increasing the thickness of the ITO film. The lowest value of sheet resistance is for the as-deposited ITO film on glass (20.8Ω/Sq., sample d5 at 10% P_{O2}). Other R_s values of the ITO films are 26.5 /Sq for sample d4, 32.5 Ω/Sq for sample d3, 85.6 /Sq for sample d2 and 99.9 Ω/Sq for sample d1 respectively. From above, the R_s of the as-deposited ITO film is sufficiently low to use it as a transparent electrode layer.

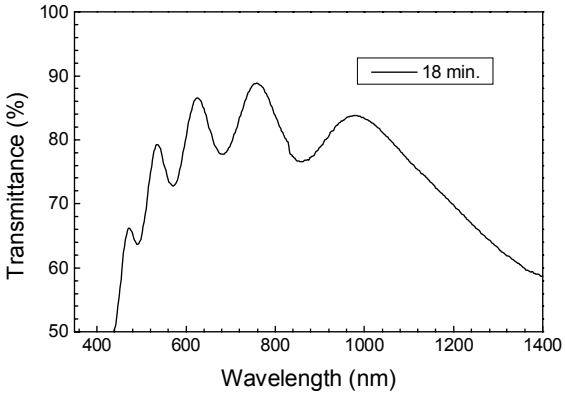


Fig. 4-5-2. Interference transmission spectrum of the ITO film (sample d5) with 18 minutes deposition time.

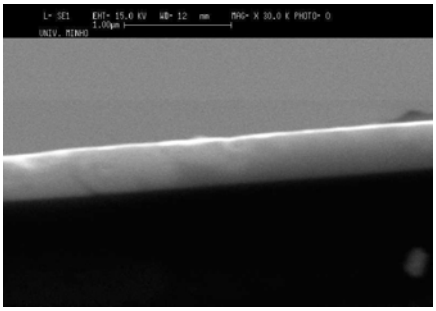


Fig. 4-5-3. SEM micrograph showing the cross section of the ITO film (sample d4) with 10 minutes deposition time.

The Figure of Merit ($\Phi_{TC}= T_{max}/R_s$) of the sample is mainly influenced by the R_s (Section 4.2.3). The data of the samples is seen in Table 4-5-1. As the thickness of the films is increased the R_s decreases (samples d1-d5), and the transmission T_{max} has no significant changes. We conclude that it is possible to deposit thin ITO films with higher Φ_{TC} by increasing film thickness while keeping other process parameters almost constant. The important micro-constants, carrier concentration (n_c) and the carrier mobility (μ) of the ITO films with different thicknesses will be discussed in Chapter 5.

4.5.3. Refractive index (n) and thickness (d)

Several authors reported detailed results about the n dispersion of the films prepared at different total pressures and P_{O2} [22, 24-25]. As the thickness of our samples d4 and d5 are thick enough for getting interference curves of the transmittance spectra, we calculated the thickness of the ITO films with Equ. (3.16). The calculated values are 488.6 nm and 793.5 nm. These values were confirmed by the SEM results. We calculated the n of the sample deposited with 10% P_{O2} at 560 nm and 785 nm wavelength by the Swanepoel method (Section 3.6); they are n=1.84 and n=1.78 respectively. The interference curve of the transmittance spectrum of sample d5 is shown in Fig. 4-5-2 and the SEM of sample d4 is shown in Fig. 4-5-3.

4.5.4. Diffuse reflectance, specular reflectance and TIS

Fig. 4-5-4 shows the DR, SR and their calculated TIS spectra over the range 300-810 nm, plotted against wavelength. The δ values based on Equ.(3.2) (Section 3.3) for all ITO films are summarized in Table 4-5-1. As seen from the Table, the surface roughness value is in the range from 11.3 to 12.9 nm. Fig. 4-5-5 shows a typical AFM

micrograph of the surface microstructure and topography of the ITO films (sample d1) that were deposited at 10% P_{O2} and 2.1×10^{-1} Pa total pressures. The nanometer surface δ and nanometer grain boundaries are clearly seen in the Figure. The grain size (diameter of the columns in the top surface) is 32 nm and the average height of δ is less than 16 nm.

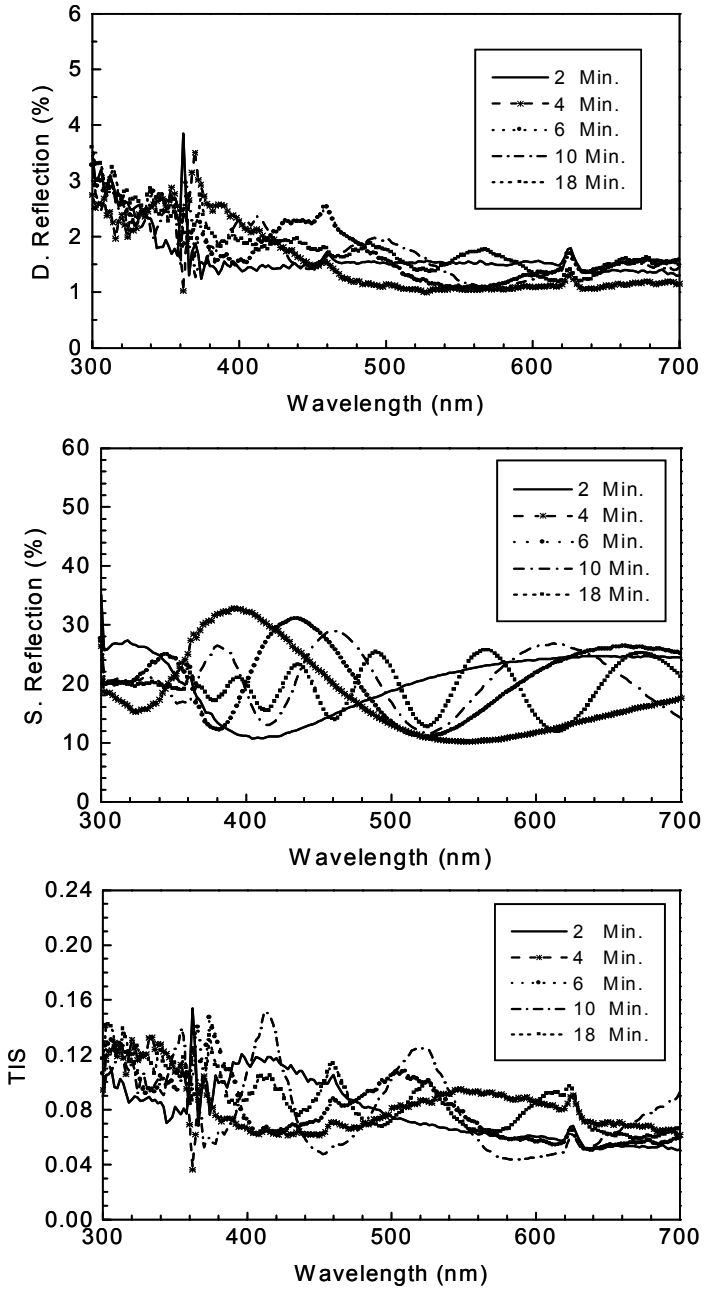


Fig. 4-5-4. (a) Diffuse reflectance, (b) Specular reflectance and (c) TIS of ITO films over a wavelength range of 300-810 nm prepared at different oxygen partial pressures (P_{O2}). Solid line: 2 Min. (d1 sample), Star line: 4 Min. (d2), Circle line: 6 Min. (d3), Dash dot line: 10 Min. (d4), Square line: 18 Min. (d5).

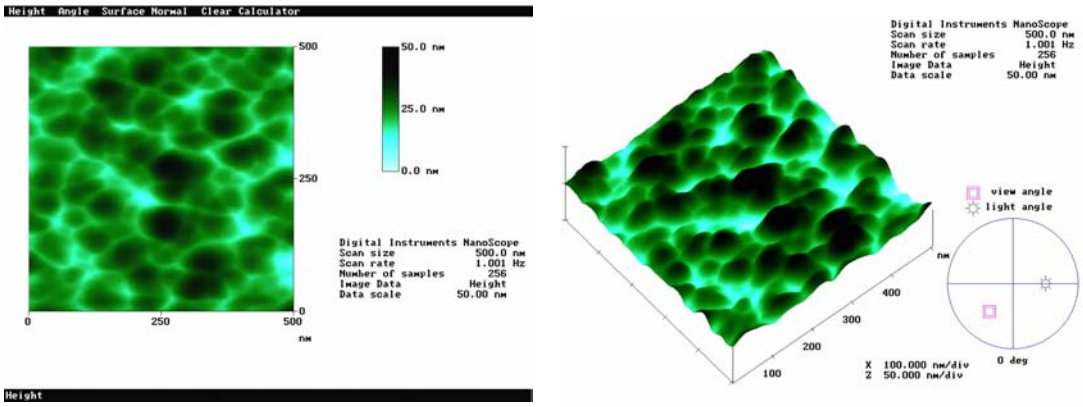


Fig. 4-5-5. AFM surface microstructure showing the roughness of an ITO film (sample d1) prepared at room temperature, 10% P_{O2} and 2.1 x 10^{-1} Pa total pressure.

4.5.5. Energy band gap E_g

The α^2 value has been plotted vs. the photon energy in Fig. 4-5-6, which was originally obtained from the measurement of the absorption spectrum (Section 3.7). Table 4-5-1 shows the E_g values of the ITO films. The obtained E_g values vary between 3.32 and 3.69 eV for different film thickness. Here we can directly use the contribution of Burstein-Moss-Shift or modified Burstein-Moss-Shift to explain the bigger E_g vlaue. The E_g of the film has a clearly tendency to decrease with the increasing of the film thickness, from sample d2 to d5. Since the thickness of the film is thin, the glass substrate has strong effect on the optical parameters of the film. The thinner the film is, the higher the optical band gap is [22].

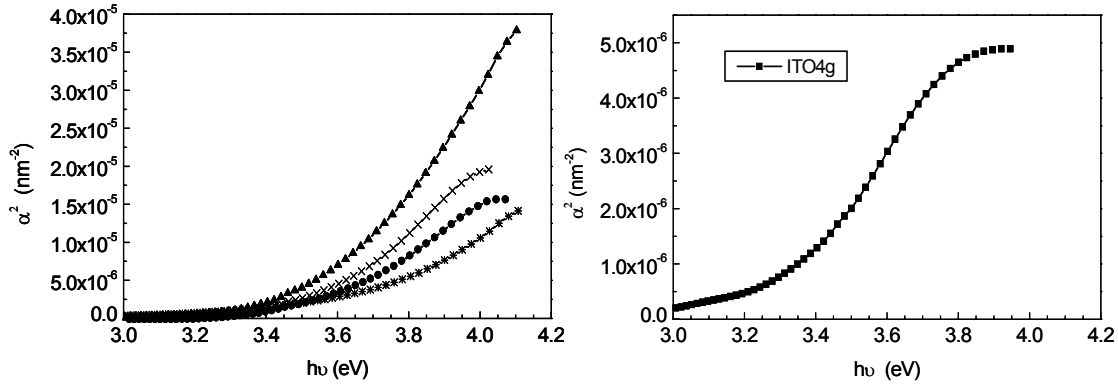


Fig. 4-5-6 Dependence of the absorption coefficient on the photo-energy. Up triangle: 2 Min., Star: 4 Min., Circle: 6 Min., Cross x: 10 Min., Square: 18 Min.

4.5.6. Microstructure of ITO film

As we know, the slope of the short wavelength edge of the transmission curve is steep or has a blue shift in accordance with a narrow distribution of particle sizes in the material. This is related to (i) The formation of ultra-fine particle (UFP) microstructure, (ii) With nanometer thickness, (iii) Having a larger crystalline/defect ratio of the film. The absorption peak (transmission onset) is due to a 1s-1s quantum particle transition as suggested by Rajeshivar [14]. A slight increase in the transmission and a slight shift of the absorption edge to a shorter wavelength had been also observed in the ultra fine particles (UFP) CdS materials [15]. The same effect is observed in Fig. 4-5-1. It is found that the onset of the spectrum of sample d5 is located at 350 nm and that of the sample d1 (300 nm) is shifted towards shorter wavelengths by 50 nm in Fig.4-5-1. This is either related to the formation of a UFP microstructure and to the nanometer size ultra thin film or to a larger crystalline/defect ratio in the thinner film (or during the beginning stage of the deposition). The slope of the edge of the transmission curve is steep, or has a blue shift in accordance with a narrow distribution of particle sizes. The results analysis shows that the grain size of the surface increases from sample d1 to d5 when the film was deposited using a longer deposition time. The AFM and SEM results confirmed this conclusion.

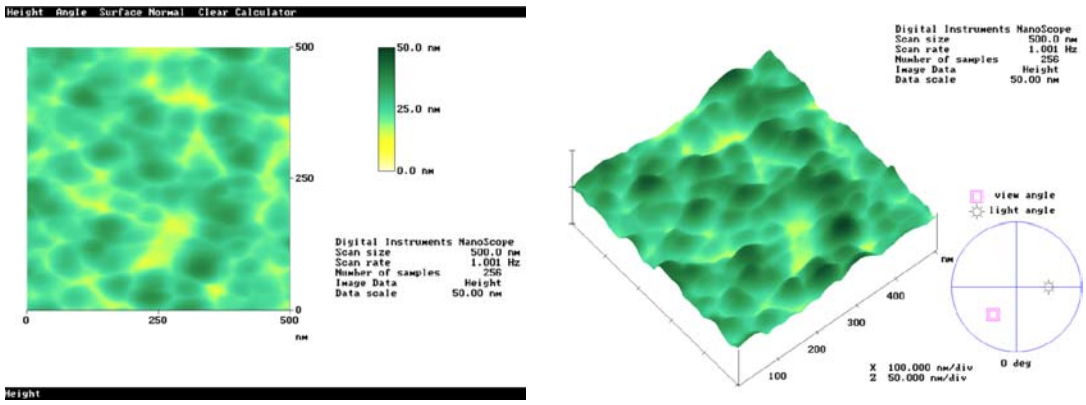


Fig. 4-5-7. AFM surface microstructure showing the roughness of an ITO film (sample d6) prepared at room temperature with 21% P_{O2} and 2.1×10^{-1} Pa total pressure.

Fig. 4-5-7 shows the typical AFM micrographs of the surface microstructure and topography of an ITO film (sample d6) that were deposited with 21% P_{O2} and 2.1×10^{-1} Pa total pressure. The nanometer surface δ and nanometer grain boundaries are clearly

seen in the Figure. The grain size is 35 nm, the average height of δ is less than 18 nm. By comparing the AFM and SEM (Fig. 5-4-8) results, we observe that the grain size increases from ~35 nm to ~ 80 nm when the film was deposited during 2 minutes and 32 minutes respectively. Also the SEM micrograph shows a gradual increase of the grain size from the bottom to the top surface of the ITO film.

From Fig. 4-5-7 and 4-5-8 we can conclude that the film structure of samples d6 and d7, deposited at the same conditions as samples d1-d5 except for 400 ^{0}C substrate temperature and 21% P_{O2}, changes from a small grain size to a slightly bigger grain size after the film thickness increases.

While the thickness of the films further increases, the surface of the film appears greyish. As shown in Fig. 4-5-8 there is a slightly bigger particle size in the surface of the films. The blackening of the ITO film was caused by the reduction of SnO_2 in the films [26, 27]. This reduction process of the ITO film can be described as $2CO + SnO_2 \Rightarrow 2CO_2 + Sn$. SnO_2 films are also used as CO sensing films and device [28, 29]. Carbon monoxide in the residual gas is related to the blackening during sputtering. The standard free energy for this reaction is a few kcal mol^{-1}. Chubachi and Aoyama [26] suggested that this reaction is possible if the CO^+ ions are accelerated by the electric field in the sheath around the substrate and impinge on the ITO surface with high energy. Fan and Bachner [30] studied the powder removed from the surface of an ITO target after sputtering. They founded that the darkest regions contain Sn rather than the In element, which results from the chemical reduction of the SnO_2 by the loss of oxygen during sputtering. This reduction process was also observed in our EDX results (Section 4.7.5). It can explain the reason of the decrease of the concentration of SnO_2 from target 10% SnO_2 to less than 6% SnO_2 in deposited film.

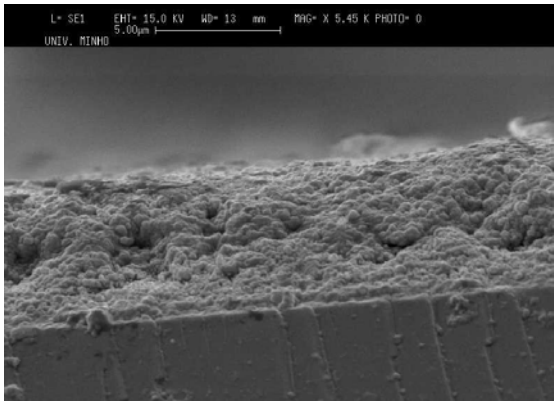


Fig. 4-5-8. SEM micrograph of a 5 µm thick ITO film, for a 32 minutes deposition time (the film of sample d7 is not transparent).

4.5.7. Conclusions of the section

The E_g of the film varies within 3.32 eV - 3.69 eV for different deposition conditions and decreases slightly as the film thickness increases from 188 nm to 846 nm. The glass substrate has a strong effect on the energy band gap E_g of the film, and makes it high. The thinner the film is, the higher the E_g is. From the transmittance spectra, AFM and SEM results we observed that the grain size gradualy increases when the film was deposited in a longer time. In case of very thin film with thickness less than 400 nm, the films have good electrical conductivity due to the increasing of thickness. The best performance of the Figure of Merit is 44.2 x 10^{-3} Ω^{-1} and was achieved in sample d5, deposited using 10% P_{O2} and 2.1x10^{-1} Pa total pressure. Sample d5 has 20.8 Ω/Sq sheet resistance, 90% maximum visible transmission at 846 nm thickness. Although the values (sample d1-d5) of transmittance and R_s are not as high as expected, no annealing makes the production process less expensive, easier to produce which is needed in some types of device applications.

4.6. Influence of "Low Temperature" Annealing on the Properties and Micro-structure of the ITO Films

As we know ITO films are extensively used in a wide variety of TCO (transparent conducting oxides) applications. The information and studies of chemical stability and properties of the films at different annealing temperatures are thus important and needed. In this section we discuss the influence of "low temperature (≤ 300 ^{0}C)" annealing on the properties and microstructure of the ITO films.

4.6.1. Sheet resistance of the films deposited in 10% P_{O2} and conductance mechanisms

Table 4-6-1 shows the properties and data of the ITO film before and after annealing in vacuum and air. The as-deposited films with 188 nm thickness yielded sheet resistance (R_s) of 121.1Ω/Sq. The R_s decreased to a value of ~64 Ω/Sq after annealing in the range of 100-200 ^{0}C in vacuum. After 200 ^{0}C annealing temperature (T_a) the R_s increased from 66.0 Ω/ Sq to 117.2Ω/Sq with increasing temperature. For the sample annealed in air there is a similar trend and the lowest R_s reached a value of ~58 Ω/Sq.

All these annealed samples had much lower R_s than that of the deposited film, except sample e7 annealed in air at 300 ^{0}C.

The difference observed between vacuum and air annealing is mainly due to the different effect of oxygen desorption. The observed decrease of R_s with annealing can be due to the associated increase in grain size and lower grain boundary scattering in the annealed films. As we know, the SnO_2 doping in the In_2O_3 films does not contribute to carrier generation in amorphous films [11, 31]. The electrical properties of pure In_2O_3 are known to rely entirely on the oxidation state of the metal constituent [32]. Since sheet resistance of pure In_2O_3 films exhibit an increase after annealing (150 ^{0}C-200 ^{0}C) [8, 33, 34], we confirmed that the deposited ITO film is not pure In_2O_3 and is In_2O_3 doped with SnO_2 from the decrease trend of R_s with annealing. It is in agreement with the EDX results, there are less 6% SnO_2 in the ITO film (section 4.7.5).

Table 4-6-1. The data and parameters of the ITO films (10% P_{O2}) annealed in vacuum and air.

Samp.	T_a(^{0}C)	R_s (Ω/Sq.) [	E_g(eV)	T_{max} (%) Vacuum / Air	δ(nm)	Φ_{max}($10^{-3}\Omega^{-1}$)]
e1	-	121.1	3.78	91	12.5	7.5
e2	80	108.0/101.4	3.77/3.71	92/94	13.1/12.5	8.5/ 9.3
e3	100	62.1/57.2	3.76/3.69	95/97	13.8/12.6	15.3/16.9
e4	150	63.8/58.1	3.75/3.68	96/97	14.2/12.6	15.1/16.7
e5	200	66.0/58.7	3.74/3.66	98/98	14.9/12.8	14.8/16.7
e6	250	86.0/128.7	3.80/3.77	98/97	14.4/12.7	11.4 /7.5
e7	300	117.2/212.4	3.87/3.85	99/96	14.0/12.7	8.4 /4.5

Symbols and abbreviations refer to Table 4-2-1, it is the reference ITO film without annealing.

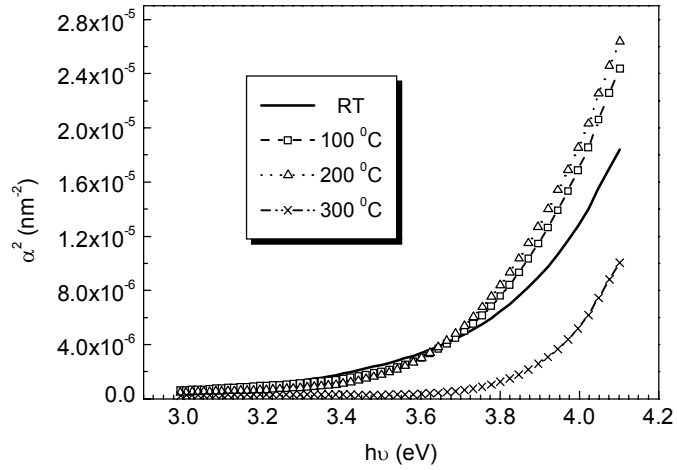


Fig. 4-6-1. Dependence of the absorption coefficient on the photo-energy. ITO films were annealed in vacuum at temperatures of 100 ^{0}C (Square), 200 ^{0}C (Up Triangle), 300 ^{0}C (Cross×). Solid line corresponds to the as-deposited film.

4.6.2. Energy band gap of the films deposited with 10% P_{O2}

E_g values were obtained from analysis of the absorption spectra at different T_a in vacuum (Fig.4-6-1). Table 4-6-1 gives E_g values that vary between 3.87 and 3.66 eV for all annealed films in vacuum and air. As the ITO samples in this work show comparably high effective band gaps, we conclude that this is caused by Burstein-Moss-Shift (Section 4.4.4).

4.6.3. Diffuse reflectance, specular reflectance and TIS of the films deposited with 10% P_{O2}

Fig. 4-6-2 shows the diffuse reflectance, specular reflectance and TIS spectra of the annealed ITO films over a range of 300-810 nm, plotted against wavelength. The δ values based on Equ. (3.2) (Section 3.3) for all samples are summarized in Table 4-6-1. As seen from the Table, the surface presents a roughness in the range from 12.5 to 14.9 nm. The roughness δ increases after annealing. The light scattering is caused by the surface δ and the grain boundaries. The typical δ of the as-deposited film was 12.5 nm. The films annealed in vacuum at more than 100 ^{0}C were rougher as indicated by higher δ values. The films are much rougher after vacuum annealing than in air annealing. Films annealed in air show almost no significant changes in the surface roughness.

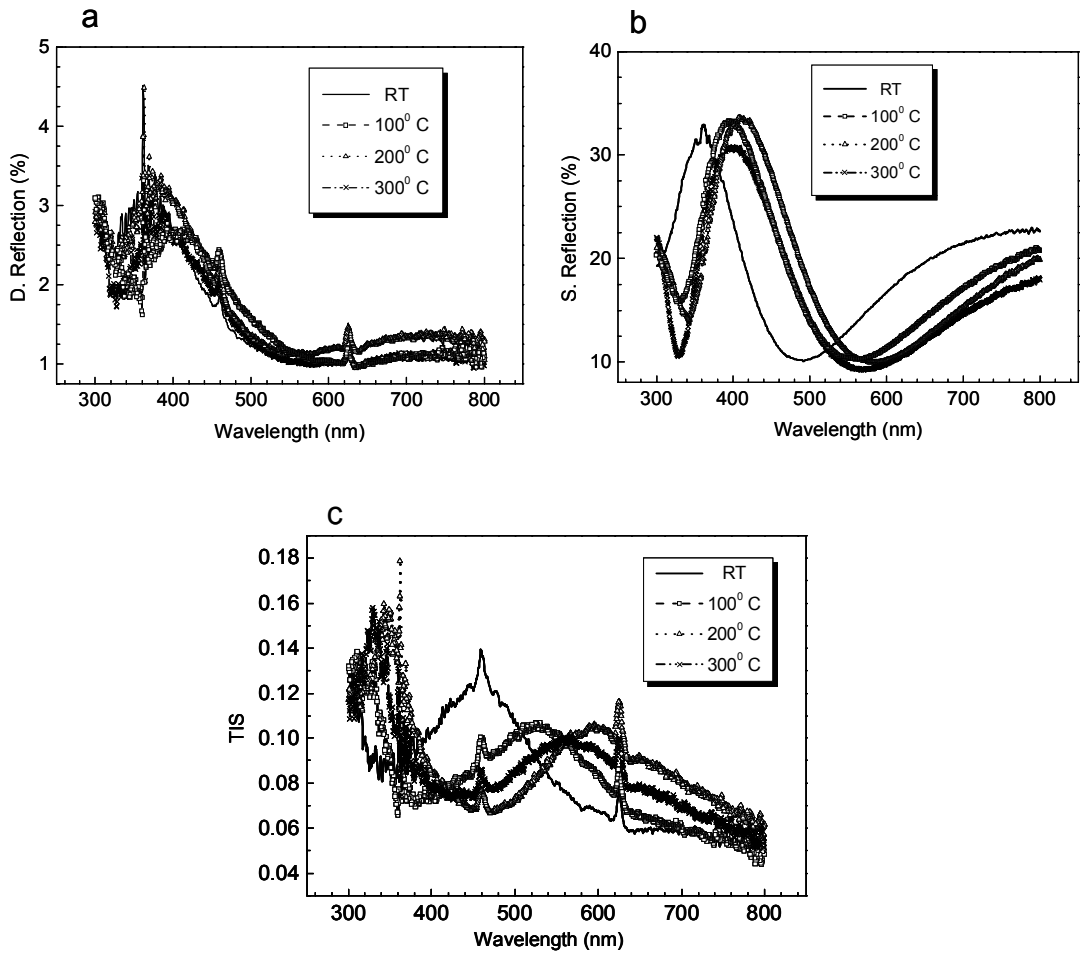


Fig. 4-6-2. (a) Diffuse reflectance, (b) specular reflectance and (c) TIS spectra of ITO films at different annealing temperatures in vacuum. Solid line: as-deposited, Square line: 100 ^{0}C, Up triangle: 200 ^{0}C, Cross x: 300 ^{0}C.

4.6.4. Transmittance of the films deposited with 10% P_{O2}

The transmission spectra of ITO films, as-deposited and annealed in vacuum, are shown in Fig.4-6-3. All transmittance data at maximum (T_{max}) is listed in Table 4-6-1. About 98 % T_{max} is achieved in the visible spectral region after annealing of 200 ^{0}C. The transmittance of ITO films increases with increasing T_a. The value of the transmission of the as-deposited ITO films is above 83% in the visible range and becomes lower in the NIR range. Fig. 4-6-3 indicates that, (i) The onset of the spectrum of the 300 ^{0}C annealed sample appears a 395 nm side absorption peak I (or the transmittance splits to II peak 350 nm and III peak 530 nm). (ii) The slope of the onset of the transmission of the annealed samples is steeper than sample e1 at room temperature (RT). (iii) The onset of the absorption split (or the maximum transmission

peak) of annealed sample shifted towards longer wavelength comparing with the sample e1. This indicates that the crystalline domain increases. A similar behavior was found in section 4.7.2 and it will be explained there. Table 4-6-1 gives the values of the Figure of Merit ($\Phi_{TC}= T_{max}/R_s$) of all the samples (R_s is sheet resistance).

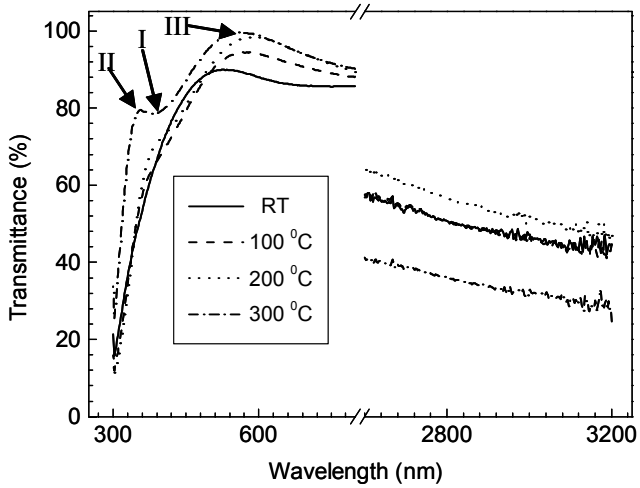


Fig. 4-6-3. Transmittance spectra of the films prepared with 10% oxygen partial pressure at different annealing temperatures in vacuum.

4.6.5. Influence of the annealing on the electrical properties of ITO films deposited with 20% and 25% P_{O2}

a. Sheet Resistance

The sheet resistance (R_s) of the ITO films, which were deposited at RT with 20% and 25% P_{O2} respectively, are shown in Table 4-6-2. The as-deposited film (sample f4) with –70 V bias deposited in 2 minutes, yielded the lowest Rs of 250.2 Ω/Sq. For this film the R_s increased sharply to 651.5 Ω/ Sq. after 200 ^{0}C T_a in vacuum. Samples f3 and f4 were deposited with total pressure of 8×10^{-2} Pa. The other samples were deposited with total pressure of 1×10^{-1} Pa. It is observed that the lower total pressure yielded smaller R_s comparing all samples f1-f4. The R_s of the film that was deposited in higher P_{O2} (20% and 25% P_{O2}) increases after annealing at 200 ^{0}C (or 300 ^{0}C) in vacuum. The bigger value of R_s is caused by decreasing the ratio of crystalline/defect under annealing temperature.

Table 4-6-2. Experimental conditions and parameters of the ITO films before and after annealing in vacuum

Samp.	P_{O2} (%)	T_d (Min.)	T_{max} (%)	R_s (Ω/ Sq.)	E_g (eV)	Φ_{max} ($10^{-3}\Omega^{-1}$)	T_a (^{0}C)	note
f1	25	2	97.1	4032.2	3.12	0.24	-	no bias
f1a	25	2	97.7	6725.6	3.49	0.15	200	no bias,
f2*	25	2	98.0	3768.2	3.54	0.26	-	no bias
f2a*	25	2	98.3	5369.1	3.53	0.18	200	no bias,
f3	20	2	95.8	257.9	3.58	3.71	-	no bias
f3a	20	2	96.4	532.0	3.10	1.8	200	no bias,
f4	20	2	95.1	250.2	3.43	3.8	-	-70V bias
f4a	20	2	96.5	651.0	3.14	1.48	200	-70V bias
f5	20	5	93.4	33.8	3.78	27.6	-	-100V bias
f5a	20	5	96.1	106.4	3.83	9.0	300	-100V bias

Note: The symbol * indicates the samples deposited with total pressure of 8×10^{-2} Pa. Other samples were deposited with total pressure of 1×10^{-1} Pa. T_a: Annealing Temperature. Other symbols and abbreviations refer to Table 4-2-1.

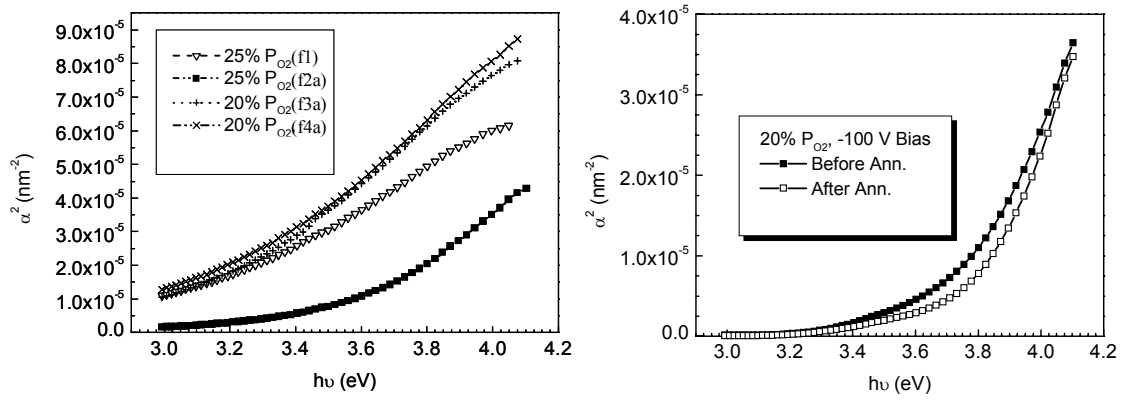


Fig. 4-6-4. Dependence of the absorption coefficient on the photo-energy. ITO films were deposited at different P_{O2}, bias voltages and with or without annealing.

b. Energy Band Gap

Table 4-6-2 gives the E_g values of all ITO films. The obtained values vary between 3.10 and 3.83 eV. The direct transition model (N=2) was chosen using $\alpha^N = C(h\nu - E_g)$ for the calculations of E_g (Section 3.7). They were obtained from absorption spectra at different P_{O2}, bias voltages and temperatures (Fig.4-6-4).

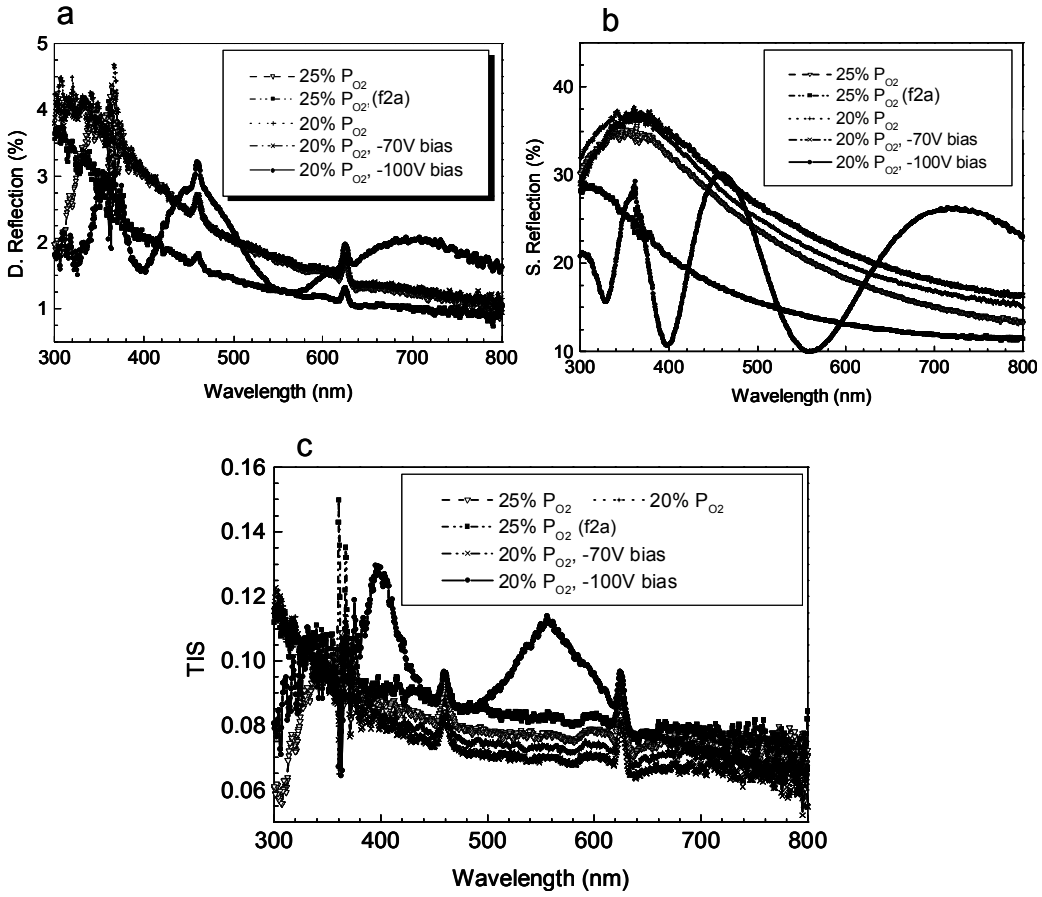


Fig. 4-6-5. (a) Diffuse reflectance, (b) specular reflectance and (c) TIS of ITO films at annealing temperature of 200 ^{0}C (or 300 ^{0}C) in vacuum.

4.6.6. Influence of annealing on the optical properties of ITO films deposited with 20% and 25% P_{O2}

a. Diffuse reflectance, specular reflectance and TIS

Fig. 4-6-5 shows the diffuse reflectance, specular reflectance and TIS of ITO films. The δ values based on Equ.(3.2) (Section 3.3) for all as deposited samples are lower than 13.7 nm. The roughness δ becomes higher (15.9 nm maximum) after annealing in vacuum.

b. Transmittance spectra

The transmittance spectra of the ITO films annealed in vacuum are shown in Fig. 4-6-6. All maximum transmittance data of the samples is listed in Table 4-6-2. About 96.4%~ 98.3 % T_{max} is achieved in the spectral region 400 nm-1500 nm after annealing in vacuum at 200 ^{0}C. The transmittance of the ITO films increases after annealing. All

the values of the transmission of the ITO films after annealing are above 87% in the range 400 nm-1500 nm except for samples fa and f5a (5 minutes deposition time, -100 V bias). This comes from its lower sheet resistance 33.8 Ω/ Sq. and it is explained by a clear increase of free electrons in the films with 100 negative bias voltage and substrate temperature [13, 16].

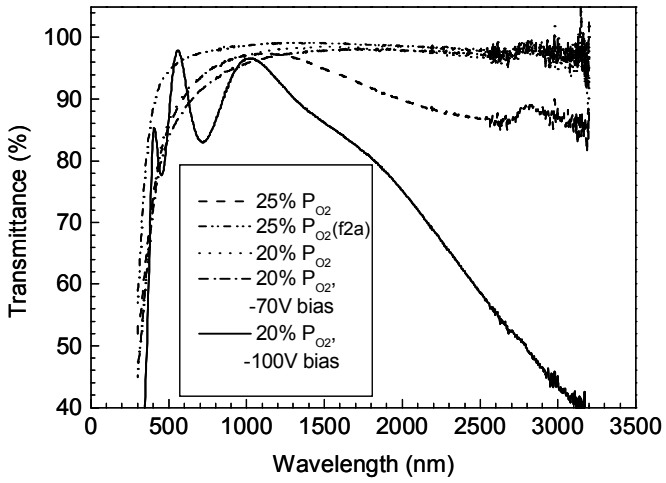


Fig. 4-6-6. Transmittance spectra of the films prepared with 20% and 25% ratio of oxygen partial pressure at 200 ^{0}C annealing temperature in vacuum.

c. Refractive index (n) and thickness (d) of the ITO film

Similar to section 4.5.3, the calculated n of the sample f5 is 1.87 at 446 nm wavelength by the method described in section 3.6. The calculated n value of sample f5a (annealing of sample f5) is 1.95 at 454 nm wavelength. We calculated the thickness of the ITO films f5 and f5a with Eq. (3.16). The calculated values are 316 nm and 300 nm respectively.

4.6.7. Conclusions of the section

We have investigated the role of "low temperature" annealing in vacuum and air on the electrical and optical properties of ITO films on glass. The results showed that the annealing affects the sheet resistance, transmittance and morphology of the ITO films.

For the films deposited with 10% P_{O2}, there are some improvements of the electrical conductivity and transparency of the films after annealing from 80 ^{0}C to 300^{0}C in

vacuum and air. The lowest R_s is 33.8 Ω/Sq and was obtained in the ITO film annealed at 100 ^{0}C in vacuum and air. At higher annealing temperatures a rapid decline in the electron conductivity occurs. The increasing of the oxygen vacancies may cause an high conductivity. The E_g varies within 3.66 eV - 3.87 eV and decreases as the annealing temperature increases from 80 to 200 ^{0}C. At 300 ^{0}C the E_g reached the biggest value (3.87 eV) in the range of annealing temperatures 80-300 ^{0}C. The films exhibited high maximum optical transmittance (99%) and high minimum transmittance (> 85 %) in the visible range (>420 nm wavelength) after annealing at 300 ^{0}C. The δ of the as-deposited film was 12.5 nm. The films annealed at more than 100 ^{0}C were rougher as indicated by higher δ values. The film is much rougher after vacuum annealing than after air annealing.

For the films deposited with 20% and 25% P_{O2}, the R_s of the film became bigger after annealing at 200^{0}C temperature in vacuum than that of the films deposited with low P_{O2} such as 10%. The lowest R_s is 33.8 Ω/Sq and was obtained for the as deposited ITO film during 5 minutes with -100 V bias. For films deposited with -70 V bias, the lowest R_s is 250.2 Ω/Sq and was obtained for the as deposited ITO film during 2 minutes. At annealing temperatures 200 ^{0}C or 300 ^{0}C a rapid decline in the electron conductivity occurred. The E_g varies within 3.10 eV - 3.83 eV. The films exhibited high maximum optical transmittance (96.5%~98.3%) after annealing at 200 ^{0}C. The maximum roughness δ is 13.7 nm before annealing and increases to 15.9 nm after annealing.

4.7. Influence of "High Temperature" Annealing on the Properties and Micro-structure of the ITO Films

In section 4.6, we discussed the influence of "low temperature (≤ 300 ^{0}C)" annealing on the properties and microstructures of the ITO films. Here we give the studies on the influence of "high temperature (> 300 ^{0}C)" annealing on the properties and microstructure of the ITO films.

4.7.1. Sheet resistance of the films

The sheet resistance (R_s) for films annealed in air is shown in Table 4-7-1. The deposited (2.1×10^{-1} Pa P_t and 10% P_{O2}) films with 188 nm thickness yielded the R_s of 121.1 Ω/Sq. The R_s decreased sharply to a value of ~60 Ω/Sq after annealing in the range 100-200 ^{0}C in air. The R_s increased to 212.4 Ω/Sq at 300 ^{0}C and 234.3 Ω/Sq at

540 ^{0}C. If T_a is above 540 ^{0}C, the R_s becomes much bigger than that of the as-deposited ITO film. The glass substrate began to deform at 620^{0}C T_a. These results show a regularity of the temperature effect to the conductivity of the films in a wider temperature range.

Table 4-7-1. The data and parameters of ITO films (10% P_{O2}) annealed in air.

Samp.	T_a (^{0}C)	R_s (Ω/Sq.)	E_g(eV)	T_{max} (%)	δ(nm)	$\Phi_{max}(10^{-3}\Omega^{-1})$
g1	25	121.1	3.78	91.2	12.5	7.5
g2	220	59.7	3.66	99.0	12.8	16.5
g3	300	212.4	3.85	96.4	12.7	4.5
g4	380	228.1	3.85	97.0	13.2	4.3
g5	460	232.4	3.86	97.2	13.5	4.2
g6	540	234.3	3.87	98.1	13.8	4.2
g7	620	∞	3.88	97.3	14.0	-
g8	700	∞	-	-	-	-

4.7.2. Transmittance of the ITO films

The transmittance spectra of the ITO films as deposited and annealed are shown in Fig. 4-7-1. The maximum transmittance (T_{max}) of the samples is listed in Table 4-7-1. A much higher T_{max} (96.4~99.0 %) was achieved in the visible spectral region after annealing. The samples g1 and g2 with lower sheet resistances show lower transmission in range 2200-3000 nm. The edge of the transmission of sample g2 in the short wavelength range has split, steep slope and blue shift after 220 ^{0}C annealing. Further the onset of the spectrum of sample g2 appears with a 400 nm side absorption peak (Ref. Section 4.6.4).

As explaination in Section 4.5.6, the slope of the edge of the transmission curve is steep or has a blue shift in accordance with a good crystalline/defect ratio in the material. This means that the crystalline/defect ratio of sample g2 becomes larger (or better) at 220 ^{0}C T_a. Thus the observed lower R_s of 59.7 Ω/Sq can be associated to the increase in the crystalline domain, and to the decrease of defects and domain boundary scattering in the annealed films. For other samples (g3-g8) the bigger R_s may be caused by the decrease of the crystalline/defect ratio after further increasing T_a.

Table 4-7-1 shows the Figure of Merit (Φ_{TC}= T_{max}/R_s) of the samples. Clearly the sample g2 has a better value.

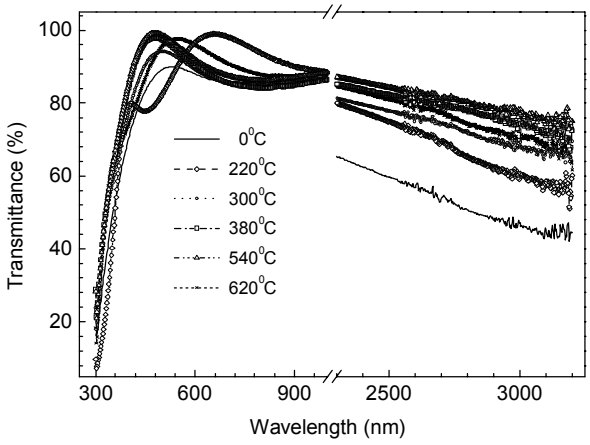


Fig. 4-7-1. Transmittance spectra of films prepared with 10% ratio of oxygen partial pressure, 2.1×10^{-1} Pa total pressure and different annealing temperatures in air.

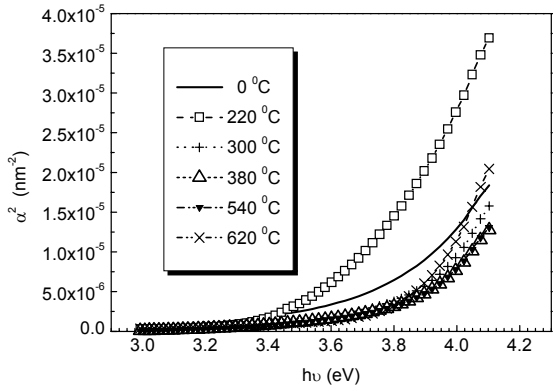


Fig. 4-7-2. Dependence of the absorption coefficient on the photo energy

4.7.3. Energy Band Gap (E_g)

Table 4-7-1 gives the E_g values, and they vary between 3.88 and 3.66 eV. They were obtained from analysis of the absorption spectrum (Fig.4-7-2). The E_g decreases as T_a increases from RT to 220 ^{0}C. The E_g increases as the T_a further increases from 300 ^{0}C to 620 ^{0}C. At 620 ^{0}C E_g reaches the biggest value (3.88 eV).

As the heat treated ITO samples show comparably high effective band gaps E_g in high temperature annealing, we conclude that a combination of Burstein-Moss-Shift and contributions of scattering causes the increased E_g (as Section 4.2.5). If the transmission increases (or shifts towards longer wavelength) in the long wavelength region (NIR), it means a decrease of free electrons in the film [13]. Because the transmission increases in

NIR region (Fig. 4-7-1), then the ΔE_{BM} value mainly comes from the contribution of broadening of scattering effect $\hbar\Sigma$.

4.7.4. Diffuse reflectance, specular reflectance and TIS

Diffuse reflectance (DR) and specular reflectance (SR) spectra were measured for different annealing temperatures of the films as a function of wavelength. The δ values based on Equ. (3.2) (Section 3.3) for all samples are summarized in Table 4-7-1. The δ for as deposited samples was 12.5 nm. The annealed film was rougher as indicated by higher δ values up to 14.0 nm. The light scattering is mainly caused by the surface roughness δ and domain size too. Domain sizes grow after annealing. The results thus showed that the annealing temperature affects the morphology of the films.

4.7.5. Structural characteristics of the ITO films

Fig. 4-7-3 shows the effect of the annealing temperature (T_a) on the XRD curves of the ITO films. An amorphous film was obtained at RT, irrespective of the SnO_2-doping concentration in the film. The ITO films prepared at low annealing T have no sharp peak in their X-ray diffraction spectra. Only a weak In_2O_3 (211) peak, and a mixed peak of In_2O_3 (222) plus broad background from the glass substrate can be observed. There is no evidence of SnO_2 peaks in the spectra. This is due to the small amount of SnO_2 in the ITO films. Our EDX results demonstrated that there are only less than 6% SnO_2 in the ITO films. EDX analysis of one region is shown in Fig. 4-7-4. The spectrum shows X-ray emissions from O (0.52 KeV), Si (1.89 KeV), a strong In (3.34 KeV) and week Sn (3.44 KeV). The reason of decrease of the concentration of SnO_2 from target 10% SnO_2 to less than 6% SnO_2 in deposited film was detailedly explained in Section 4.5.6. Briefly it is thought that the reaction of SnO_2 and residual gas CO causes the loss of SnO_2, also possibly the lack of the oxygen during the process is another reason.

No clear change was observed in the XRD spectrum on the annealed films at temperatures lower than 250 ^{0}C. However, after annealing in air at 300 ^{0}C for 1 hour, sharp In_2O_3 (211), (222), (400), (411), (431), (440), (611), (622) and (800) peaks emerged on the XRD. The films have (222) and (400) plane structure mainly. The better poly-crystallisation was observed from the change in the predominant plane of crystallisation (222) and (400) planes after annealing. It demonstrates that the annealing of the ITO film is of much better polycrystalline structure.

From the above discussion the minimum of R_s at T_a lower than 300 ^{0}C is not due to the phase transformation of the ITO films [8, 35], because the XRD pattern did not show differences below 300 ^{0}C. The study of CdS films had a similar result [8]. The existence of a minimum R_s after annealing is a well known behaviour of ITO (10 wt % SnO_2-doped In_2O_3), But for the In_2O_3 film with 6% SnO_2 doped this only happens for annealing below 250 ^{0}C. If the annealing T is above 300^{0}C , R_s becomes higher than that of the as-deposited ITO films again, because these In_2O_3 with 6% SnO_2 have mainly characteristic of In_2O_3 (Section 4.6.1).

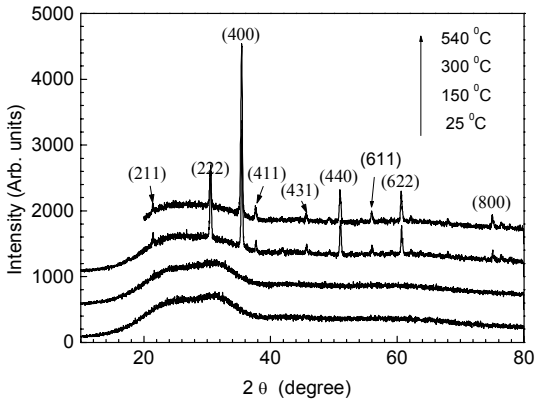


Fig. 4-7-3. XRD patterns of ITO films on glass substrates at different annealing temperatures (RT-540 ^{0}C).

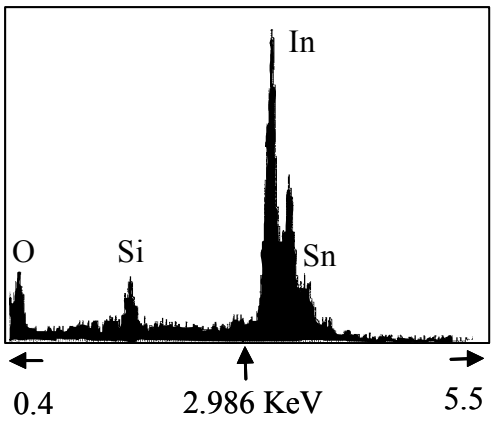


Fig. 4-7-4. The region of EDX spectrum of an ITO film on glass substrate.

4.7.6. Conclusion of the section

Room temperature growing of ITO films and high temperature post-annealing up to 700 ^{0}C were studied. After the heat treatment in air there are some changes of the electronic conductivity, transparency and micro-structure characteristics.

The lowest R_s (59.7 Ω/Sq.) was obtained for ITO films annealed at 220 ^{0}C in air. Above 300 ^{0}C a rapid decline in the electronic conductivity occurred. Small crystalline/defect ratio (causing strong scattering of carriers) and severe loss of oxygen vacancies causes the higher R_s. The E_g value varies in range of 3.66 eV-3.88 eV. The E_g increases as T_a further increases from 300 ^{0}C to 620 ^{0}C. The results showed that T_a affects the morphology of the ITO films. A minimum surface roughness of 12.5 nm was obtained at RT. The film surface becomes rougher up to 14.0 nm as T_a is increased. The treated films exhibited a better maximum transmittance (96.4~99.0 %) in the visible range.

The as deposited films are amorphous. A better crystallisation was observed from the change in the predominant plane of crystallisation (222) and (400) plane after heat treatments. Sharp (211), (222), (400), (411), (431), (440), (611), (622) and (800) peaks of In_2O_3 emerged in XRD at 300 ^{0}C annealing in air for 1 hour. The film with improved R_s after low T annealing (less than 250 ^{0}C) is still amorphous. Our EDX results demonstrated that there are only less than 6% SnO_2 in the ITO films. The film annealed at 220 ^{0}C is suitable for EC smart window application or other functional multilayer film applications.

4.8. Summary of the Chapter

In this chapter we presented the study of the transparent and conductive ITO (indium-tin-oxide) films deposited on glass by dc sputtering. The variation of the film properties with $P_{02,}$ bias voltage, substrate temperature and post annealing temperature were analysed. Detailed information on the transmittance, absorption, diffuse reflectance and specular reflectance were given. The surface roughness (δ), thickness, sheet resistance and energy band gap (E_g) of the ITO films were obtained in order to characterize the film microstructures and properties.

The sheet resistance (R_s) below 100 Ω/Sq was obtained for the ITO film, which deposited in 10% P_{O2} plus with bias voltage (from -70 to -100 V) or post-annealing temperature at 100-200 ^{0}C or substrate temperature (200- 400 ^{0}C). For the optimum sample, the film has more than 95% maximum transmission and 35.0×10^{-3} Ω^{-1} Figure of Merit (Φ_{max}) at ~100.0 nm thickness. From spectra calculation, AFM photography and AFM software analysis, the surface roughness δ of the ITO film was obtained. All surface roughness values are lower than 18 nm.

The as-deposited ITO films at room temperature are amorphous. A better crystallisation was observed from the change in the predominant plane of crystallisation (222) and (400) plane after heat treatment. Sharp In_2O_3 (211), (222), (400), (411), (431), (440), (611), (622) and (800) peaks emerge in XRD for 300 ^{0}C annealing in air (1 hour). Depending on the application, both amorphous and polycrystalline ITO films are obtained by controlling the deposition conditions. In the case of target composition 10% SnO_2 doped In_2O_3, our EDX results demonstrated that there are only less than 6% SnO_2 in the ITO films. The reason of decrease of the concentration of SnO_2 from target

10% SnO_2 to less than 6% SnO_2 in deposited film was explained. It is thought that the reaction of SnO_2 and residual gas CO causes the loss of SnO_2, also possibly due to the lack of the oxygen during the process maybe is another reason.

The energy band gap E_g varies within 3.26 eV - 3.86 eV. The high values of E_g of the films under consideration compared to the intrinsic E_g could be explained by Burstein-Moss-Shift or a modified Burstein-Moss-Shift. The glass substrate has also a strong effect on the E_g of the films, and makes it high. The thinner the film is, the higher the E_g is.

Table 4-8-1. Comparison of ITO films prepared by different methods and researchers.

Technique	Resistivity (Ωcm)	T_{Max} % (region)	Thickness (nm)	T_s (^{0}C)	Ref.
dc sputter	5.4x 10^{-4}	94% (560nm)	282	RT	This Work
dc sputter	~1.0x 10^{-3}	85% (visible)	-	RT	[36]
rf sputter	6.3x 10^{-5}	89% (visible)	1400	380	[37]
rf sputter	3.7x 10^{-4}	87% (visible)	900	400	[38]
rf sputter	1.9x 10^{-2}	92% (visible)	40	RT	[9]
E-beam	3.0x 10^{-4}	92% (visible)	150	350	[39]
Ion&E-beam	5.1x 10^{-4}	90% (550nm)	120	RT	[40]
R-evapor	7.0x 10^{-4}	80% (visible)	-	200	[41]
Pulse-laser	4.0x 10^{-4}	90% (750nm)	-	RT	[42]
Sol-Gel	9.5x 10^{-4}	90% (900nm)	250	260	[43]
Spray pyroly	5.0x 10^{-3}	85-90% (visible)	200-900	350-500	[44]
Thermal	9.1x 10^{-4}	80% (visible)	120	80	[45]

Note
Max: Maximum; ***dc sputter:*** dc Magnetron sputtering; ***E-Beam:*** Electron beam evaporation; ***R-evapor:*** Reactive evaporation; ***Pulse-laser:*** Pulsed laser deposition; ***Spray pyroly:*** Spray pyrolysis; ***Thermal:*** Thermal deposition; ***Region:*** Spectrum region in nm; ***RT:*** room temperatura.

From the transmittance spectra, AFM and SEM the grain size of the surface gradually increases when the film was prepared in a longer time, heated substrate and post-annealed. There is much improvement in the visible transmittance of the films after heating and annealing. All data of the Chapter is important for industrial production or further applied research in related field. The comparison of ITO films prepared by different methods and researchers is shown in table 4-8-1. The prepared ITO films (dc sputtering method using ceramic target) were compared with commercial ITO films under work operations. The photograph of optical transparence and electric conductivity between home-made and Commercial ITO are showed in Fig. 4-8-1. They show similar characteristics and properties. The films, which are deposited at RT and annealed at temperature lower than 220 ^{0}C, heated less than 220 ^{0}C to substrate and with negative

bias, suit applications of EC smart windows or other applications of functional multilayer films.

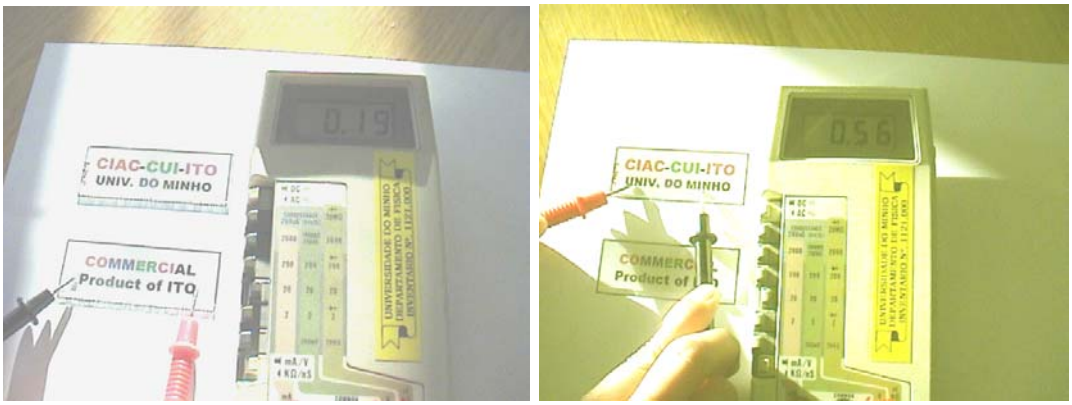


Fig. 4-8-1. Photograph showing the optical transparence and electric conductivity between home-made and commercial ITO

4. 9. References

[1] A. L. Dawar. J. C. Joshi, Mater. Sci. 19 (1984) 1.

[2] I. Hamberg and C. C. Granqvist, J. Appl. Phys. 60(11) (1996) 123.

[3] T. J. Vink, W. Walrave. J. L. C. Daams, P. C. Baarslag, and J. E. A. M.van der Meerakker, Thin Solid Films 266 (1995) 145.

[4] P. Song, Y. Shigesato, I. Yasui, C. W. Ow-Yang, and D. C. Paine, Jpn.J. Appl. Phys., Part 1, 37 (1998) 1870.

[5] F. O. Adurodija, H. lzurni, T. lshihara, H. Yoshioka, and M. Motoyama, J. Vac. Sci. Technol. A 18(3) (2000) 814.

[6] J. Machet, J. Guile, P. Saulnier and S. Robert , Thin Solid Films 80 (1981) 149.

[7] S. Takaki, K. Matsumoto, and K. Suzuki, Appi. Surf. Sci. 33/34 (1988) 91.

[8] Hai-Ning Cui and Shi-Quan Xi, Thin Solid Films 288(1996)325-329.

[9] C. Nunes de Carvalho, G. Lavareda, E. Fortunato, A. Amaral. "Properties of ITO films deposited by r.f.-PERTE on unheated polymer substrates—dependence on oxygen partial pressure". Thin Solid Films, 427 (2003) pp. 215-218.

[10] S. Naseem, I. A. Rauf, K. Hussain, N. A. Malik, Effects of oxygen partial pressure on the properties of reactively evaporated thin films of Indium oxide, Thin Solid Films 156 (1988) 161.

[11] D. C. Paine, T. Whitson, D. Janiae, R. Beresford, and C. O. Yang, A study of low temperature crystallization of amorphous thin film indium-tin-oxide, Appl. Phys. 85 (1999) 8445-8450.

[12] R. Groth, Phys. Status Solidi, 14(1966)69.

[13] M. Bender, W. Seelig, C. Daube. H. Frankenberaer . B. Ocker. J. Stollenwerk, Thin Solid Films 326 (1998) 72-77.

[14] Rajeshwar K., Adv. Mater. 4 (1992) 23

[15] Cui H-N, Wang R., Wang W. Y. and Xi S. Q. Preparation and photo-luminescence of ultrafine cadmium sulfide particles, J. of Mat. Sci. Lett. 17(11) (1998) 913-916.

[16] T. S. Moss, Optical Properties of Semiconductors, Butterworths Inc. (London), (1959).

[17] Milton Ohring, The Materials Science of Thin Films, Academic Press Inc.(San Diego), (1992) P.454

[18] Kyu-Hyun Kim, Kyoon Choi, Eui-Seok Choi, Jin-Ha Hwang and Jeung-Tae Hwang, Indium tin oxide thin films deposited by RF-magnetron sputtering for organic electro-luminescence devices, Journal of Ceramic Processing Research. Vol. 4, No. 2, pp. 96~100 (2003) 。

[19] Ray S, Banerjee R, Basu N, Batabyal A K, Barua A K., J. Appli. Phys., 54 (1983) 3497.

[20] E. Burstein, Phys. Rec., 93 (1954) 632.

[21] C. H. L. Weihtens and P. A. C. Van Loon, Thin Solid Films, 196 (1991) 1.

[22] L.-J. Meng, M.P. Santos, Vacuum 45 (1994) 1191.

[23] P. Gao, L. J. Meng, M. P. dos Santos, V. Teixeira, M. Andritschky, Vacuum 56 (2000) 143.

[24] http: //windows. lbl.gov/materials/chromogenics: optical indices of electrochromic material on ITO.

[25] Gao, P., L.J. Meng, M. P. dos Santos, V. Teixeira, M. Andritschky, "Influence of sputtering power and the substrate-target distance on the properties of ZrO2 films prepared by RF reactive sputtering" Thin Solid Films, 377, 557 (2000)

[26] Chubachi Y, Aoyama K. Jpn. J. Appl. Phys. 30 (1991) 1442.

[27] Matsuoka T, Kuwata J, Fujita Y. Abe A. Jpn. J. Appl. Phys. 27 (1988) L1199.

[28] J. Miguel Correia-Pires, Vasco Teixeira, J. Borges de Almeida, Nanostructured Materials and Coatings for Biomedical and Sensor Applications, Kluwer Academic Publishers, Ed. Y.G. Gogotsi and I.V. Uvarova, (2003), p. 343-355

[29] J. M. Correia-Pires, J. B. Almeida, V. Teixeira, "Gas sensitive response of SnO_2 thin film sensors produced by reactive DC magnetron sputtering", Key Engineering Materials 230-232 (2002) p.388-391

[30] Fan J. C. C, Bachner F. J., J. Electrochem. Soc. 122 (1975) 1719.

[31] Y. Shigesato and D. C. Paine, Appl. Phys. Lett. 62 (1993) 1268.

[32] R. B. H. Tahar, T. Ban, Y. Ohya, and Y. Takahashi, J. Appl. Phys. 83 (1998), 2631.

[33] A. Monteiro, M. F. Costa, B. Almeida, V. Teixeira, J. Gago, E. Roman, Structural and Optical Characterization of WO_3 Deposited on Glass and ITO, Vacuum 64 (2002) 287.

[34] T. Minami, H. Sonohara, T. Kakumu, S. Takatu, Thin Solid Films, 270 (1995) 37.

[35] Hiroshi Uda, Seiji Ikegami and Hajimu Sonomura, Jpn. J. Appl. Phys., 29(1) (1990), 30.

[36] S. Bhagwat, R.P. Howson, Use of the magnetron-sputtering technique for the control of the properties of indium tin oxide thin films, Surface and Coatings Technology 111 (1999) 163–171.

[37] D. Mergel, M. Schenkel, M. Ghebre, M. Sulkowski , Structural and electrical properties of In 2O3 :Sn films prepared radio-frequency sputtering,Thin Solid Films 392(2001)91-97.

[38] Li-Jian Meng, M.P. dos Santos, Properties of indium tin oxide films prepared by rf reactive magnetron sputtering at different substrate temperature, Thin solid Films, 322(1998) 56-62.

[39] Joseph George, C.S. Menon, Electrical and optical properties of electron beam evaporated ITO thin films, Surface and Coatings Technology 132 (2000) 45-48.

[40] J. W. Bae, J. S. Kim, G. Y. Yeom, Indium-tin-oxide thin film deposited by a dual ion beam assisted E-beam evaporation system, Nuclear Instruments and Methods in Physics Research B, 178 (2001)311-314.

[41] J. Ma, D. H. Zhang, J. D. Zhao, C. Y. Tan, T. L. Yang, M. L. Ma, Appl. Surf. Sci. 151(3-4) (1999)239.

[42] V. Craciun, D. Craciun, Z. Chen, J. Hwang, R.K. Singh, Room temperature growth of indium tin oxide thin films by ultraviolet-assisted pulsed laser deposition, Applied Surface Science 168 (2000) 118-122.

[43] M. J. Alam, D. C. Cameron, Characterization of transparent conductive ITO thin films deposited on titanium dioxide film by a sol-gel process, Surface and Coatings Technology, 142-144 (2001) 776-780.

[44] E. Benamar, M. Rami, C. Messaoudi, D. Sayah, A. Ennaoui, Structural, optical and electrical properties of indium tin oxide thin films prepared by spray pyrolysis, Solar Energy Materials and Solar Cells 56 (1999) 125–139.

[45] A. Salehi, Thin Solid Film, 324 (1, 2) (1998)214.